

Aged organic aerosol in the Eastern Mediterranean: the Finokalia Aerosol Measurement Experiment – 2008

L. Hildebrandt¹, G. J. Engelhart¹, C. Mohr², E. Kostenidou^{3,4}, V. A. Lanz², A. Bougiatioti⁵, P. F. DeCarlo², A. S. H. Prevot², U. Baltensperger², N. Mihalopoulos⁵, N. M. Donahue¹, and S. N. Pandis^{1,3,4}

¹Center for Atmospheric Particle Studies, Carnegie Mellon University, 5000 Forbes Ave., Pittsburgh, PA, 15213, USA

²Laboratory of Atmospheric Chemistry, Paul Scherrer Institut, 5232 Villigen, Switzerland

³Institute of Chemical Engineering and High Temperature Chemical Processes (ICE-HT), Foundation of Research and Technology (FORTH), Patra, Greece

⁴Department of Chemical Engineering, University of Patras, Patra, Greece

⁵Environmental Chemical Processes Laboratory (ECPL), University of Crete, Heraklion, Greece

Received: 18 December 2009 – Published in Atmos. Chem. Phys. Discuss.: 22 January 2010

Revised: 16 April 2010 – Accepted: 27 April 2010 – Published: 5 May 2010

Abstract. Aged organic aerosol (OA) was measured at a remote coastal site on the island of Crete, Greece during the Finokalia Aerosol Measurement Experiment-2008 (FAME-2008), which was part of the EUCAARI intensive campaign of May 2008. The site at Finokalia is influenced by air masses from different source regions, including long-range transport of pollution from continental Europe. A quadrupole aerosol mass spectrometer (Q-AMS) was employed to measure the size-resolved chemical composition of non-refractory submicron aerosol (NR-PM₁), and to estimate the extent of oxidation of the organic aerosol. Factor analysis was used to gain insights into the processes and sources affecting the OA composition. The particles were internally mixed and liquid. The largest fraction of the dry NR-PM₁ sampled was ammonium sulfate and ammonium bisulfate, followed by organics and a small amount of nitrate. The variability in OA composition could be explained with two factors of oxygenated organic aerosol (OOA) with differing extents of oxidation but similar volatility. Hydrocarbon-like organic aerosol (HOA) was not detected. There was no statistically significant diurnal variation in the bulk composition of NR-PM₁ such as total sulfate or total organic aerosol concentrations. However, the OA composition exhibited statistically significant diurnal variation with more oxidized OA in the afternoon. The organic aerosol was highly oxidized, regardless of the source region. Total OA concentrations also

varied little with source region, suggesting that local sources had only a small effect on OA concentrations measured at Finokalia. The aerosol was transported for about one day before arriving at the site, corresponding to an OH exposure of approximately 4×10^{11} molecules cm⁻³ s. The constant extent of oxidation suggests that atmospheric aging results in a highly oxidized OA at these OH exposures, regardless of the aerosol source.

1 Introduction

Fine atmospheric particles can scatter or absorb radiation, as well as influence cloud formation and lifetime, and therefore affect climate (IPCC, 2007). They also affect human health by, among others, damaging the respiratory and cardiovascular systems (Dockery et al., 1993; Davidson et al., 2005; Pope and Dockery, 2006). Organic aerosol (OA) globally comprises a significant fraction (20–90%) of the submicron particle mass (Kanakidou et al., 2005; Zhang et al., 2007). While the formation of inorganic aerosol is relatively well understood (Seinfeld and Pandis, 2006), organic aerosol is not. In contrast to fine-mode inorganic aerosol, which is mostly composed of a few well-characterized components such as sulfates, nitrates and ammonium, organic aerosol is composed of thousands of species, many of them unidentified (Goldstein and Galbally, 2007). In addition, OA has a myriad of sources – both anthropogenic and biogenic, particle-phase and gas-phase. Furthermore, OA is dynamic:



Correspondence to: S. N. Pandis
(spyros@andrew.cmu.edu)

most of its components are semi-volatile and can evaporate, can be transported and further processed in the atmosphere, and can re-partition to the aerosol phase (Robinson et al., 2007). Even though much progress has been made in recent years, both the formation and the evolution of OA remain poorly understood.

From a source perspective, organic aerosol can be classified as fresh primary (POA), oxidized POA (OPOA) or secondary organic aerosol (SOA) (Donahue et al., 2009). In this classification, POA refers to compounds that are emitted as particles and have not reacted in the atmosphere. OPOA is formed when POA is oxidized, either by heterogeneous oxidation or when POA evaporates as it is diluted during transport (Lipsky and Robinson, 2006) and the resulting vapors are oxidized, reducing their volatility and allowing them to re-condense on existing particles (Robinson et al., 2007). SOA is formed when volatile or intermediate volatility organic compounds (VOCs or IVOCs) undergo one or more chemical transformations in the gas phase, forming less volatile compounds that then partition to the particle phase (Chan et al., 2009; Hallquist et al., 2009; Hildebrandt et al., 2009; Presto et al., 2009). After formation, SOA as well as POA can re-evaporate and be further oxidized and transported in the atmosphere. This additional gas-phase oxidation appears to be principally responsible for most of the “aging” of organic aerosol (Lambe et al., 2009). Aging and transport can result in elevated OA concentrations far away from sources, contributing to the regional nature of the fine-mode aerosol problem. Air-quality models tend to under-predict the concentrations of OA in the atmosphere, especially in the summer when photochemical activity is high (Volkamer et al., 2006; Goldstein and Galbally, 2007; Karydis et al., 2007), suggesting that we do not understand the aging of OA well.

Recent advances in aerosol mass spectrometry and factor analysis allow us to also separate OA based on its bulk chemical characteristics. Typical resulting classes include a reduced component (hydrocarbon-like organic aerosol, HOA), a biomass burning component (BBOA), and a more oxidized component (oxygenated organic aerosol, OOA) (Zhang et al., 2007). Most of the organic aerosol mass is OOA: in urban areas, OOA comprises on average 60% of the organic PM_{10} (particulate matter smaller than 10 μm in diameter), while in remote areas in the absence of large sources (e.g. biomass burning), OOA often exceeds 90% of organic PM_{10} (Zhang et al., 2007; Morgan et al., 2010). OOA can frequently be further separated into highly oxygenated OA, now referred to as low-volatility OOA (LV-OOA), and less oxygenated OA referred to as semi-volatile OOA (SV-OOA) (Jimenez et al., 2009; Ng et al., 2010; Ulbrich et al., 2009). Fresh POA corresponds closely to HOA; OOA is generally associated with oxidation products in the particle phase: OPOA or SOA. While AMS factor analysis cannot usually distinguish between OPOA and SOA, the source types of OPOA (emitted as particles) and SOA (emitted as gases) are often

different, and hence the distinction is useful for the development of policy actions.

Laboratory data suggest that the oxygen-to-carbon ratio (O:C) of organic aerosol, which approximates the extent of oxidation of the OA and can be estimated from AMS measurements, increases as the aerosol is exposed to atmospheric oxidants (Grieshop et al., 2009b; Sage et al., 2008). Organic aerosol in the atmosphere also appears to be dynamic and evolves from more reduced OA to more oxidized OA (Zhang et al., 2007; Capes et al., 2008; DeCarlo et al., 2008; Morgan et al., 2010; Ng et al., 2010). The objective of this work is to improve our understanding of atmospheric processing of OA by characterizing aged OA at a remote site.

The Finokalia station is located in the northeast of the island of Crete, Greece. It is far away from anthropogenic sources and influenced by air masses from different source regions (Mihalopoulos et al., 1997; Sciare et al., 2003; Koulouri et al., 2008). The chemical compositions of the fine particle mass ($PM_{1.3}$ – particles smaller than 1.3 μm in diameter) and coarse particle mass ($PM_{10-1.3}$ – particles larger than 1.3 μm but smaller than 10 μm in diameter) at Finokalia have been characterized with 1–3 day time resolution over a 2-year period from July 2004 to July 2006 (Koulouri et al., 2008). In the summer, $PM_{1.3}$ was composed mostly of inorganic salts (60%) and organic material (30%), with small contributions from elemental carbon, dust and water. The inorganic mass was found to be mostly ammonium sulfate and ammonium bisulfate. Factor analysis showed that $PM_{1.3}$ could be explained by five factors, identified based on the loadings of various chemical components. Two factors were natural (crustal and marine) and three factors were anthropogenic (heavy oil combustion, transportation, and secondary aerosol). Considering the absence of industrial plants close to the site, the presence of aerosol from heavy oil combustion suggests influence of long-range transport of pollution from continental sites (Koulouri et al., 2008).

The above studies greatly enhanced our understanding of the sources and composition of aerosol particles in the Eastern Mediterranean. However, the lower time-resolution characteristic of filter samples precludes analysis of changes in aerosol composition by time of day, and it also limits the ability to observe changes by source region. Furthermore, the filter OC analysis technique only allows for a total mass measurement of organic carbon and does not provide information on the extent of oxidation of the organic aerosol. In the present study, we employ a quadrupole aerosol mass spectrometer (Q-AMS, or AMS) to characterize the non-refractory submicron particle mass (NR- PM_{10}) (Jayne et al., 2000; Jimenez et al., 2003; Canagaratna et al., 2007). The AMS measures NR- PM_{10} in real time and thereby avoids potential problems that may arise when collecting, transporting and storing filter samples. The AMS complements other aerosol characterization techniques such as filter samples in that it allows us to:

- 1) Measure the size-resolved composition of NR-PM₁ at high time resolution.
- 2) Study the organic aerosol mass spectrum, its underlying components and its approximate oxidative state.
- 3) Investigate the variation in the aerosol composition with photochemical conditions (time of day) and source region of the aerosol.

Previous campaigns combined airborne measurements of particles and gases, measurements from ships and measurements at land-based stations including Finokalia, and they showed that measurements at Finokalia are representative of the background Eastern Mediterranean atmosphere (Kouvarakis et al., 2002; Lelieveld et al., 2002). As such, this study provides insights about aerosol in the Eastern Mediterranean as well as the transport and evolution of organic aerosol in general.

2 Experimental

2.1 Sampling site

Measurements were conducted at the Finokalia Station of the Environmental Chemical Processes Laboratory of the University of Crete. The station is located at a remote coastal site in the northeast of the island Crete, Greece, in the Eastern Mediterranean (35°20' N, 25°40' E, 150 m above sea level). It is located 50 km east of Heraklion, the most populous city of the island, and 400 km southwest of Athens, the closest megacity. The nearest settlement is a small village of 10 inhabitants, about 3 km south of the station. A more detailed description of the site has been published elsewhere (Mihalopoulos et al., 1997), and the meteorological conditions during this specific study are described by Pikridas et al. (2010).

2.2 Measurement campaign

The measurements were conducted during the Finokalia Aerosol Measurement Experiment-2008 (FAME-2008), which was part of the EUCAARI intensive campaign during May 2008 (Kulmala et al., 2009). An overview of the measurements and results of FAME-2008 (Pikridas et al., 2010) and a detailed analysis of the organic aerosol volatility (Lee et al., 2010) are presented in companion publications. Here, we shall focus on results from the AMS measurements, especially the composition and characteristics of the organic aerosol.

2.3 Instrumentation and methods

The size-resolved chemical composition of the aerosol was measured using a Q-AMS from Aerodyne Research, Inc. (Jayne et al., 2000; Jimenez et al., 2003; Canagaratna et al.,

2007). The particles were not dried before sampling. The particle number distribution was monitored using a scanning mobility particle sizer (SMPS, TSI model 3034). The volatility of OA was measured using a thermodenuder system built based on the design of An et al. (2007). A number of other measurements were performed during this campaign. Of particular interest to this study are PM₁ filter samples, which provided a separate measure of the concentration of inorganic and organic aerosol; a steam sampler (Khlystov et al., 1995), which provided an additional measure of the concentration of inorganic aerosol; and nephelometers, which measured aerosol light scattering. Other instruments present at the site during FAME-2008 included a rotating drum impactor for measuring metals (Bukowiecki et al., 2009, and references therein), aethalometers (aerosol light absorption) and gas monitors for NO_x, CO and CO₂. Meteorological data (temperature, relative humidity, wind speed and direction, etc.) are also available. A summary of the measurements from most of these instruments is presented by Pikridas et al. (2010).

2.3.1 Q-AMS

The Q-AMS alternated operation between mass spectrum (MS) scanning mode and particle time-of-flight (pToF) mode every fifteen seconds. The sample averaging time was set at three minutes, and further averaging was performed in the post-analysis of the data. The vaporizer temperature was set at 600 °C to ensure fast and complete vaporization of the ammonium sulfate. The AMS measures only non-refractory (NR) PM₁, i.e. compounds that flash-vaporize at the heater temperature of 600 °C. It does not measure refractory material such as black carbon, sea salt and silica (dust). Considering that previous measurements have determined that most (~90%) of the fine particle mass (PM_{1,3}) at Finokalia is non-refractory (Koulouri et al., 2008) and that sea salt and silica are mostly present at the larger sizes in the PM_{1,3} range, the fact that the AMS cannot measure refractory species is expected to affect total PM₁ measurements by less than 10% and is therefore not a large concern.

Quantification of aerosol concentrations measured by the AMS is challenging due to incomplete transmission of larger particles (>~400 nm vacuum aerodynamic diameter) through the high-throughput aerodynamic lens and particle bounce at the vaporizer. We estimated the AMS collection efficiency (CE) for these data by matching AMS mass distributions and SMPS volume distributions using the OA density and AMS CE as fitting parameters (Kostenidou et al., 2007), as described in more detail in our companion paper (Lee et al., 2010). Fitting the distributions up to approximately 500 nm mobility diameter minimizes the importance of the tail of the distributions where both of the instruments are less reliable. This method does not allow us to separate the effects of particle transmission through the lens and particle bounce

at the vaporizer; hence, the estimated CE may account for both effects.

The AMS provides three separate measures of the NR-PM₁ that are used in this analysis: the chemical composition, the total mass spectrum from which the organic mass spectrum is derived, and the aerosol size distribution based on the vacuum aerodynamic diameter (Canagaratna et al., 2007). The collected data were analyzed using a standard AMS fragmentation table and batch table (Allan et al., 2004), with a few modifications. These modifications, as well as details on the calibration of the AMS and correction of the data for ambient humidity are explained in Appendix A.

The relative organic spectra are the contributions of the organic fragments at each m/z to the total organic mass. The mass fragments at m/z 44 mostly correspond to the CO₂⁺ ion (Aiken et al., 2008) and can therefore be used as a semi-empirical measure of the extent of oxidation in the system. Aiken et al. (2008) have shown that the fraction of organic mass at m/z 44, $f_{44}=[m/z\ 44]\ (\mu\text{g m}^{-3})/C_{\text{OA}}\ (\mu\text{g m}^{-3})$, where C_{OA} is the total mass concentration of the organic aerosol, can be used to estimate the oxygen to carbon ratio (O:C) in the organic aerosol. They found significant correlation between O:C and f_{44} described by the following least-squares fit:

$$\begin{aligned} (\text{O}:\text{C}) &= (3.82 \pm 0.05) \cdot f_{44} + (0.0794 \pm 0.0070), \quad (95\% \text{CI}) \\ R^2 &= 0.84 \end{aligned} \quad (1)$$

This correlation was primarily derived from ambient measurements in Mexico City, so the applicability to the data presented here is uncertain. However, it will nevertheless provide an estimate of the O:C ratio of the OA measured at Finokalia, and f_{44} is expected to be correlated with the extent of oxidation of the OA.

Aiken et al. (2008) also found a significant correlation between the ratio of organic mass to organic carbon (OM:OC) and O:C. This relationship was found to be applicable to field data as well as laboratory data and is described by:

$$\begin{aligned} (\text{OM}:\text{OC}) &= (1.260 \pm 0.002) \cdot (\text{O}:\text{C}) + (1.180 \pm 0.001), \\ R^2 &= 0.997 \end{aligned} \quad (2)$$

Thus, we can use the observed f_{44} to estimate O:C (O:C₄₄ – “O:C estimated by f_{44} ”) and OM:OC₄₄ of the organic aerosol measured at Finokalia.

In addition to the fragments at m/z 44, we will also focus on the fragments at m/z 43 and m/z 57. In ambient air, the fragments at m/z 43 are often primarily C₂H₃O⁺ with a smaller contribution from C₃H₇⁺. In ambient studies close to sources, the fragments at m/z 57 are often primarily C₄H₉⁺ with a smaller contribution from singly-oxidized species such as C₃H₅O⁺. For example, in Riverside CA, a mass spectrum from the late afternoon shows approximately 2/3 of the signal at m/z 57 due to the non-oxidized fragment (DeCarlo et al., 2006). Hence, f_{43} is often used as a proxy for moderately oxidized organic aerosol and f_{57} is used as

a proxy for fresh, hydrocarbon-like organic aerosol (Zhang et al., 2005a, b; Aiken et al., 2009). At a remote site such as Finokalia, the signals at m/z 43 and m/z 57 may be mostly due to oxidized ions. In any case, a low signal at m/z 57 is indicative of low or no contribution from HOA, and the relative abundance of ions at m/z 43 and m/z 44 are indicative of the extent of oxidation of the OA.

2.3.2 Thermodenuder

Changes in organic aerosol composition with moderate heating and evaporation, as well as OA volatility, were analyzed using a thermodenuder system based on the design described by An et al. (2007). In brief, aerosol passes alternately through the thermodenuder, heated to a predefined temperature, or a bypass line. The aerosol flow direction is controlled by two 3-way valves. Activated charcoal is used in the cooling stage to absorb the organic vapors and thereby avoid recondensation onto the particles. The aerosol is sent through the same sampling line to the SMPS for online measurement of the particle size distribution and to the Q-AMS for real-time measurement of the particle chemical composition. The volatility of the organic aerosol and changes in its composition are determined by comparing the residual aerosol after the thermodenuder to the ambient aerosol that was passed through the bypass line. The SMPS data is used to correct for number losses in the thermodenuder. The details of the volatility analysis are presented by Lee et al. (2010). Here, we will focus on the effect of aerosol heating and evaporation on the relative organic aerosol spectrum measured by the Q-AMS.

2.3.3 Other measurements

A steam sampler ion chromatograph was used to measure water-soluble inorganic ions. Water soluble gaseous species were removed before detection (see Pikridas et al., 2010 for details).

Daily PM_{1,3} and PM_{1,3–10} filter samples were collected using a virtual impactor (Loo, 1988). For the analysis of inorganic ions, filters were extracted with nanopure water and water-soluble ions were measured by conductivity detectors (see Pikridas et al., 2010 for details).

Carbonaceous material was analyzed from PM₁ collected daily on quartz fiber filters. Elemental and organic carbon (EC and OC) was measured from these filters using a thermal–optical transmission method and a carbon analyzer (Pikridas et al., 2010).

Two nephelometers (Radiance Research Integrating Nephelometer, Model M903) were used to measure light scattering coefficients of the aerosol. The nephelometers were kept under a weatherproof sunshade in order to ensure that operation was under ambient temperature, which was monitored at the inlet of each instrument. One nephelometer measured the scattering coefficient at ambient relative humidity

(average RH=46%), while the second nephelometer was connected to a diffusion drier and measured at lower RH (average RH=19%).

2.3.4 Categorization by source region

We categorized the air masses based on their source region using the potential emission sensitivity values (PES) of the footprint residence time plots from the FLEXPART model (Stohl et al., 1998). The details of this analysis are described in a companion paper (Pikridas et al., 2010) and more details on PES values can be found in Seibert and Frank (2004). The resulting categories, named by the region from which the air masses seemed to originate, are: marine, Africa, Athens, Greece and other continental. Athens and Greece were separated from other continental regions in order to investigate whether it is possible to detect the signature of the closest megacity or the closest continental region (Greece) at the field site.

2.3.5 Diurnal patterns: analysis of statistical significance and characterization

We conducted one-way ANOVA tests for total bulk concentrations (organics, sulfate, ammonium and nitrate), f_{43} , f_{44} , and organic aerosol factors (PMF, Sects. 2.3.6 and 3.2.3) as dependent variables, and time of day as the independent variable. ANOVA tests determine whether there are statistically significant differences in the mean values of the dependent variables (Atkinson-Palombo et al., 2006). While ANOVA tests determine the statistical significance of variation by time of day, they cannot quantify or characterize the diurnal cycle. Thus, we also conducted harmonic analysis (Wilks, 1995; Atkinson-Palombo et al., 2006) to characterize the diurnal cycle.

In brief, the general harmonic function is given by:

$$y_t = \bar{y} + C_k \cos(2\pi t/n - \phi_k) \quad (3)$$

where t is the time (1–24 in the diurnal analysis presented here), \bar{y} is the mean of the time series (e.g. y_t is the mean value of f_{44} during hour t , \bar{y} is the mean value for the whole campaign), C_k is the amplitude of the k^{th} harmonic, n is the period ($n=24$ here) and ϕ is the phase. Using only the first harmonic, the amplitude of the diurnal cycle can be estimated by (Wilks, 1995):

$$C_1 = [A_1^2 + B_1^2]^{1/2} \quad (4)$$

where

$$A_1 = 2/n \cdot \sum y_t \cos(2\pi t/n) \quad (5a)$$

$$B_1 = 2/n \cdot \sum y_t \sin(2\pi t/n) \quad (5b)$$

The phase is given by:

$$\phi_1 = \tan^{-1}(B_1/A_1) \pm \pi \quad \text{if } A_1 < 0 \quad (6a)$$

$$\phi_1 = \tan^{-1}(B_1/A_1) \quad \text{if } A_1 > 0 \quad (6b)$$

$$\phi_1 = \pi/2 \quad \text{if } A_1 = 0 \quad (6c)$$

The portion of the variance explained by the first harmonic, analogous to a correlation coefficient (R^2) commonly computed in regression analysis, is given by

$$V_1 = [(2/n) \cdot A_1^2] / [(n-1) \cdot s^2] \quad (7)$$

where s is the standard deviation of the n values.

The amplitude describes the magnitude of the diurnal cycle. The phase describes to what extent the observed cycle is offset from a standard cosine curve.

2.3.6 Positive matrix factorization of organic aerosol

We applied positive matrix factorization (PMF; Paatero and Tapper, 1994) to the organic aerosol data measured by the AMS. The PMF2 algorithm (version 4.2) by P. Paatero was used to solve the bilinear unmixing problem as described below. PMF has proven useful in the analysis of ambient organic aerosol data, and details of the mathematical model, its application, output evaluation, and factor interpretation have been described elsewhere (Lanz et al., 2007, 2009; Ng et al., 2010; Ulbrich, 2009). A key assumption is that the measured dataset can be separated into a number of constant components (here, AMS mass spectra) contributing varying concentrations over time. The problem is represented in matrix form by:

$$\mathbf{X} = \mathbf{GF} + \mathbf{E} \quad (8)$$

where \mathbf{X} is an $m \cdot n$ matrix of the measured data with m rows of average mass spectra (number of time periods= m) and n columns of time series of each m/z sampled (number of m/z fit= n). \mathbf{F} is a $p \cdot n$ matrix with p factor profiles (constant mass spectra), \mathbf{G} is an $m \cdot p$ matrix with the corresponding factor contributions, and \mathbf{E} is the $m \cdot n$ matrix of residuals. \mathbf{G} and \mathbf{F} are fit to minimize the sum of the squared and uncertainty-scaled residuals (Paatero and Tapper, 1994).

3 Results and discussion

3.1 Bulk chemical composition from the Q-AMS

Figure 1 shows the chemical composition of the dry NR-PM₁ measured by the AMS as a function of time, as well as the campaign average contributions of the different aerosol components to the total aerosol mass (inset). Over the course of the campaign, total dry NR-PM₁ concentrations measured by the AMS ranged from 2 $\mu\text{g m}^{-3}$ to 24 $\mu\text{g m}^{-3}$; the average was 9 $\mu\text{g m}^{-3}$. The periods of relatively high aerosol concentrations at this remote site are due to transport of pollution. The largest fraction of the sampled aerosol was ammonium sulfate and ammonium bisulfate, followed by organics and a very small contribution from nitrate. This is in contrast to

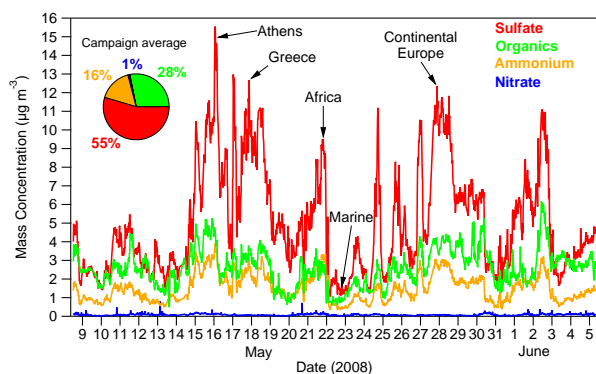


Fig. 1. Time series (9-min averages) of total mass concentrations of dry, non-refractory (NR) PM_{10} measured by the AMS and the campaign average composition (inset). The average dry NR- PM_{10} concentration was $9 \mu\text{g m}^{-3}$. Source labels point to examples of air masses from different regions.

most other regions in Europe, where the concentrations of organic aerosol are observed to be 1.5–2 times larger than those of sulfate (Morgan et al., 2010). The inorganic molar ratio $\text{NH}_4^+/(2\text{-SO}_4^{2-} + \text{NO}_3^-)$ measured by the AMS was 0.82 on average with a standard deviation of 0.09, suggesting that the aerosol was acidic most of the time. (A molar ratio of 1 corresponds to neutral aerosol; a ratio smaller than 1 corresponds to acidic aerosol.) Nitrate measured by the AMS may include organic nitrates, but since the measured nitrate concentrations were always low, the exclusion of nitrate in the inorganic molar ratio does not change it significantly. Filter measurements of the coarse particles showed that there was more nitrate in the larger particles, mostly in the form of sodium nitrate (Pikridas et al., 2010). Figure 1 also indicates some time periods when the aerosol was influenced by different source regions.

Analysis of variance (ANOVA) revealed no statistically significant variation by time of day for OA concentrations ($p = 0.12$), sulfate concentrations ($p = 0.30$) or ammonium concentrations ($p = 0.81$). Nitrate concentrations measured by the AMS revealed possibly significant variation by time of day ($p = 0.04$); however this variation appeared random and did not follow a specific diurnal pattern. The lack of diurnal variation in the bulk aerosol composition measured by the AMS is partially a result of the absence of local sources close to the field site. The production of the aerosol occurs far away from the site, and concentrations measured at the site may be more dependent on the aerosol source region and the meteorological conditions along its trajectory than on time of day and the local photochemical conditions.

Figure 2 presents the campaign average, chemically-resolved AMS particle time-of-flight (pToF) spectra of the ambient aerosol. The modes of the different aerosol species (organics, sulfate, ammonium and nitrate) are at similar diameters, suggesting that the submicrometer particles sam-

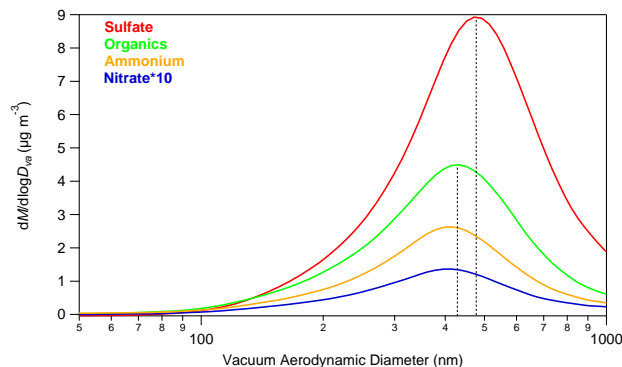


Fig. 2. The campaign average ambient particle time-of-flight size distributions of the different aerosol species measured by the AMS versus vacuum aerodynamic diameter. Dashed black lines are located at the peaks of the organic and the sulfate size distributions (430 nm and 470 nm, respectively) and are included to guide the eye. Submicrometer particles sampled during FAME-2008 had similar composition.

pled during FAME-2008 had rather similar composition. This is consistent with remote sources of the aerosol and with atmospheric processing and mixing before sampling at Finokalia. The sulfate distribution is slightly shifted to the right of the others. This could be due to slower vaporization times of sulfate and to changes in the sulfate/OA ratio over the course of the campaign: During periods of higher NR- PM_{10} concentrations, sulfate/OA was usually higher and the size of the particles was often larger. This moves the sulfate distribution to the right of the organic distribution when averaging over the whole campaign. This has only a small effect; aerosol composition was rather homogeneous with size.

The estimated collection efficiency (CE) of the ambient aerosol in the AMS was 0.85 ± 0.08 (the estimated CE of the denuded aerosol was 0.76 ± 0.09). The CE for this data set is significantly higher than the standard CE of 0.5 used in most studies. One reason for this difference may be that, in other studies, the aerosol is often dried before sampling with the AMS. Drying the particles may change the physical state of the particles from liquid to solid, which may result in increased particle bounce on the vaporizer, decreasing CE (Matthew et al., 2008). The aerosol sampled during FAME-2008 was highly hygroscopic: the aerosol mass was mostly inorganic and often slightly acidic, and the organic fraction was highly oxidized (Sect. 3.2). The ambient particles always contained some water, suggesting that they were in a liquid state, potentially leading to more efficient sampling and higher CE. The estimated CE is corroborated by the agreement between the CE-adjusted concentrations from the AMS and measurements from other instruments.

Comparison to other instruments

In Fig. 3a, we compare corrected daily averaged AMS sulfate measurements to the $PM_{1.3}$ filter measurements (slope=1.09, $R^2=0.95$) and to steam sampler data (slope=0.97, $R^2=0.79$). In order to compare the organic mass (OM) measurements from the AMS to the organic carbon (OC) measurements from the filters, we use an OM:OC ratio of 2.2, estimated using the correlations developed by Aiken et al. (2008) presented in Sect. 2.3.1 and the campaign-average f_{44} of 18.2% (Sect. 3.2.1). The resulting comparison of organic mass measured by the AMS and that measured by the filters is shown in Fig. 3b (slope=1.1, $R^2=0.78$). The corrected AMS data and the filter data agree well.

The light scattering coefficient of particles is expected to correlate with total particle mass concentration. Thus, we can also use the data from the nephelometer to further check the AMS measurements. Figure 4 shows that the scattering coefficient of dried aerosol measured by the nephelometer correlates well with the dry aerosol mass concentration from the AMS ($R^2=0.71$). The slope of the orthogonal distance regression ($2.8\text{ m}^2\text{ g}^{-1}$) is equivalent to the mass scattering efficiency. The small intercept of $2.0\times 10^{-6}\text{ m}^{-1}$ may be caused by the smaller size cut-off of the SMPS and the AMS compared to the nephelometer. In addition, considering that the aerosol was highly hygroscopic, the particles measured by the nephelometer may have contained some water even though a diffusion drier was used upstream of the nephelometer. A more thorough comparison of the AMS and nephelometer data, estimating the aerosol light scattering coefficient from the AMS chemical composition and aerosol size distribution, will be presented in a future publication.

In summary, after applying several corrections as explained in Appendix A and correcting the AMS data for the CE estimated as explained by Lee et al. (2010), the AMS data agree well with data from filters and reasonably well with data from a nephelometer. We estimate that the corrected mass concentrations from the AMS are quantitative to within 30%, consistent with previous estimates of the uncertainty in AMS measurements (Bahreini et al., 2009, auxiliary material).

3.2 Organic aerosol composition from the Q-AMS

3.2.1 High OH exposures produce highly oxidized organic aerosol

The relative organic mass spectrum from the AMS did not change appreciably over the course of the campaign, despite the influence of different source regions. Figure 5 shows 1-h averages of f_{43} , f_{44} and f_{57} as a function of time during the campaign. The organic aerosol was highly and almost uniformly oxidized (high f_{44}) throughout the campaign. The average f_{44} of 18.2% corresponds to an $O:C_{44}$ of 0.8 and an $OM:OC_{44}$ of 2.2 using the correlations introduced in

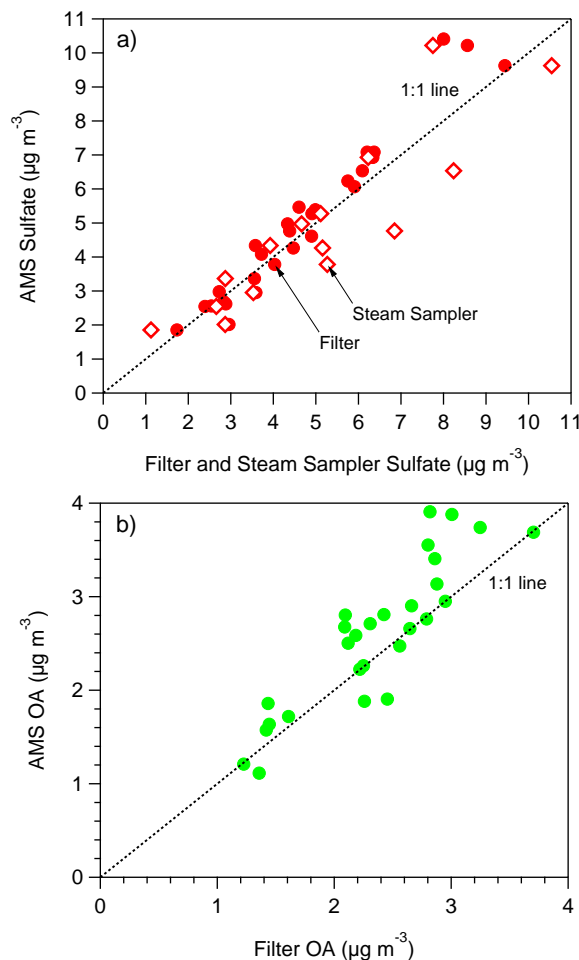


Fig. 3. (a) AMS sulfate measurements versus measurements from filters (slope=1.09, $R^2=0.95$) and a steam sampler (slope=0.97, $R^2=0.79$). (b) AMS organic aerosol (OA) measurements versus filter measurements (slope=1.1, $R^2=0.78$) using $OM:OC=2.2$. The AMS measurements agree well with filter measurements.

Sect. 2.3.1. After studying backward trajectories from the HYSPLIT model (NOAA), we estimate that it takes approximately 1 day of atmospheric processing for the aerosol to reach this highly oxidized state. This is consistent with observations of increasing O:C and aging measured by aircraft studies in Mexico City (DeCarlo et al., 2008; Jimenez et al., 2009). In order to obtain an order of magnitude estimate of the OH exposure corresponding to 1 day of atmospheric aging, we use correlations developed from measurements taken at Finokalia during the Mediterranean Intensive Oxidant Study (MINOS) in the summer of 2001 (Berresheim et al., 2003). OH levels in the Eastern Mediterranean during the summer are extremely high, reaching maximum values greater than 2×10^7 molecules cm^{-3} (Berresheim et al., 2003). We also use data on j_{NO_2} , the photolysis rate of NO_2 , which was measured during MINOS and FAME-2008.

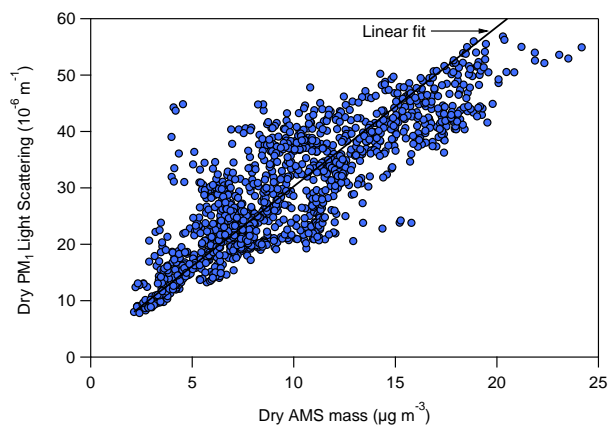


Fig. 4. Comparison of the scattering coefficient of dry PM₁ (nephelometer) to the dry AMS mass (9-min averages). Orthogonal distance regression to the data yields a slope of $2.8 \text{ m}^2 \text{ g}^{-1}$, equivalent to the mass scattering efficiency, and a small intercept of $2.0 \times 10^{-6} \text{ m}^{-1}$.

More details on this estimate can be found in Appendix B. We estimate that 1 day of atmospheric aging during FAME-2008 corresponds to an OH exposure of approximately $4 \times 10^{11} \text{ molecules cm}^{-3} \text{ s}$. Our results suggest that this exposure is sufficient to drive OA from various source regions, which probably have different POA/SOA splits initially, to this highly oxidized state.

In order to obtain insights on how quickly the increase in f_{44} occurs, we compared f_{44} in aerosol masses from similar source regions but with different transport times before detection at the site. Estimating the age of the organic aerosol is challenging, especially since we do not know when and where along a trajectory the aerosol was emitted. We will evaluate the OA age in more detail in a future modeling study. Here, we shall approximate the age as follows: using HYSPLIT trajectories, we estimate the minimum atmospheric processing time (MAPT) of aerosol as the amount of time between detection at the site and when the trajectory last passed over a continent. As a case study, consider the OA measured at 17:00 local standard time on 23 May and at the same time on 24 May. On both days, the aerosol arrived from the north-west; however, on 23 May it bypassed Greece (the last contact with a continent was Italy), whereas on 24 May it passed over Greece and Italy. For the aerosol on 23 May, MAPT was 33 h (corresponding to an approximate OH exposure of $8 \times 10^{11} \text{ molecules cm}^{-3} \text{ s}$) and $f_{44}=22\%$. On 24 May, MAPT=15 h (approximate OH exposure of $4 \times 10^{11} \text{ molecules cm}^{-3} \text{ s}$) and $f_{44}=19\%$. Twice the OH exposure results in only a slightly higher f_{44} . A similar trend was observed at other times during the campaign. While this is only a rough estimate it indicates that, under the highly oxidative conditions observed during FAME-2008, additional increase of f_{44} is relatively slow: aerosol that appears to be much older exhibits only slightly higher

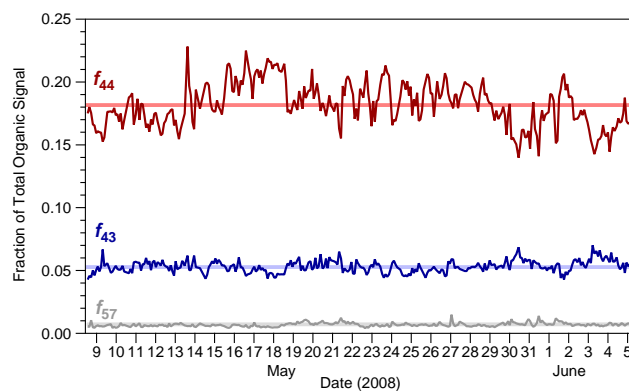


Fig. 5. Time series of one-hour averages of f_{43} , f_{44} and f_{57} in the ambient aerosol. The average of f_{44} was 18.2% (horizontal red band; $\sigma=2\%$), the average of f_{43} was 5.3% (horizontal blue band) and the average of f_{57} was 0.7% (horizontal grey band), consistent with highly aged organic aerosol.

f_{44} . This is unlike the results of laboratory experiments, where an OH exposure of $4 \times 10^{10} \text{ molecules cm}^{-3} \text{ s}$ (a factor of 10 lower than in the FAME-2008 example) has resulted in an f_{44} increase from 5% to 12% in aged Diesel OA (Sage et al., 2008) and an f_{44} increase from 4% to 8% in aged woodsmoke OA (Grieshop et al., 2009a, b). The slow increase in f_{44} observed during FAME-2008 is also different from the generally rapid photochemical processing of OA on a regional scale observed by Morgan et al. (2010) and in this study: after only 1 day of aging, the OA is very processed and highly oxidized. The seemingly slow further oxidation of aged OA could be due to fragmentation of organic compounds, which becomes more important at higher O:C (Kroll et al., 2009). When compounds fragment upon oxidation, they may volatilize, thereby slowing the oxidation of the ensemble organic material in the particulate phase.

The difference in the relative organic mass spectrum of the denuded versus the ambient aerosol also did not vary much over the course of the campaign. Figure 6 shows 12-h averages of the fractional change of f_{43} and f_{44} in the thermodenuder (TD) compared to the ambient aerosol which was passed through the bypass (BP) line, e.g. $(f_{43,\text{TD}} - f_{43,\text{BP}})/f_{43,\text{BP}}$, when the thermodenuder was operated at 97–117 °C centerline temperature. The fractional change appears to be close to zero throughout the campaign. A possible exception is during 19–21 May, when the air mass originated from Africa. This time period also exhibited the highest elemental carbon concentrations of the campaign (Pikridas et al., 2010), suggesting that the air mass was influenced by major cities in Africa. Thus, the OA measured during this time period may have been fresher than the OA measured at other times during the campaign. This is the only time during the campaign when the behavior of the OA composition in the thermodenuded aerosol versus the ambient aerosol is consistent with the inverse relationship between f_{44} and volatility

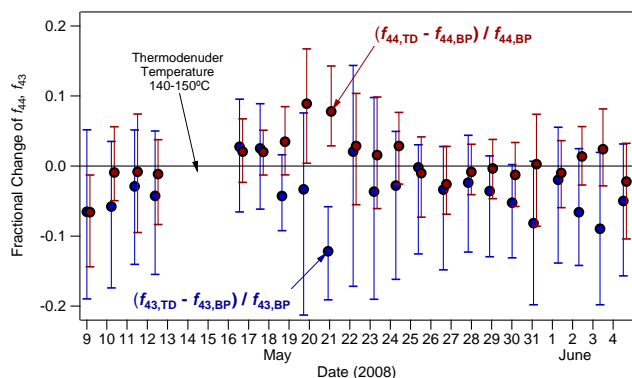


Fig. 6. Time series of 12-h averages of the fractional change of f_{43} and f_{44} in the ambient aerosol compared to the thermodenuded aerosol with the thermodenuder at 97–117 °C centerline temperature. The bars indicate the 25th and 75th percentiles. The f_{44} data are slightly off-set in the horizontal direction from the f_{43} data for improved legibility of the figure. The fractional change was close to zero throughout the campaign, with the exception of 19–21 May, when the air mass was probably influenced by major cities in Africa and possibly contained the freshest organic aerosol sampled during the campaign.

discussed below.

3.2.2 Average relative organic spectra and insights into f_{44} vs. volatility

Considering the limited variation in the organic aerosol over the course of the campaign, we now focus on the averaged mass spectra to explore the overall behavior and characteristics of organic aerosol sampled during FAME-2008. The campaign average relative organic spectra from the AMS are shown in Fig. 7 for $12 \leq m/z < 100$, which comprised over 99% of the organic mass. Error bars are the averaged standard errors calculated by the method of Allan et al. (2003), using the standard Q-AMS data analysis software (v1.41). The average relative organic spectrum of the ambient aerosol (light green sticks, grey error bars) closely resembled the relative organic spectrum of the thermodenuded aerosol (orange dots, black error bars), when the thermodenuder was operated at 97–117 °C centerline temperature (Fig. 7a). At these temperatures, the heating in the thermodenuder caused about half of the total OA mass to evaporate. At higher thermodenuder temperatures (140–150 °C, Fig. 7b), when about 3/4 of the total OA mass was evaporated, the relative organic mass spectra in the ambient and in the thermodenuded OA had small differences. For example, f_{44} in the thermodenuded, less volatile aerosol was lower than in the ambient aerosol; however, the difference is not statistically significant ($n = 109$, $t = -1.5$, $p = 0.14$), and we conclude that the thermodenuded and the ambient organic aerosol had approximately the same composition.

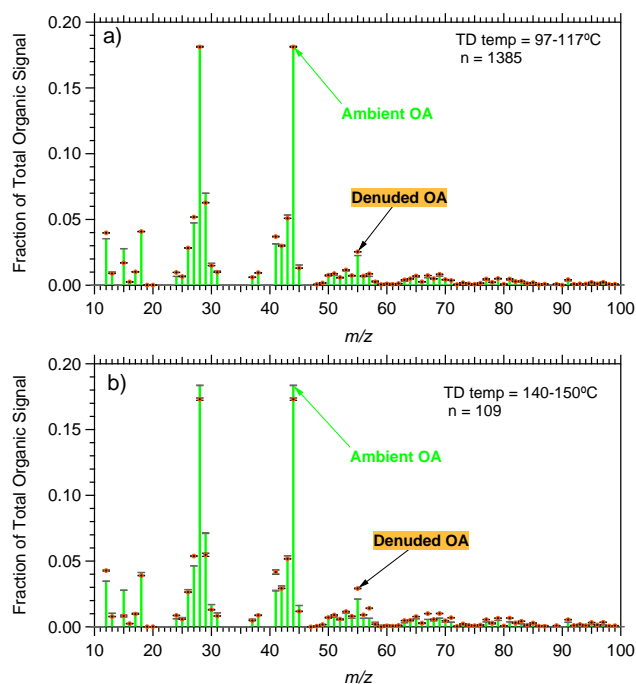


Fig. 7. The average relative organic spectra of the ambient and the thermodenuded organic aerosol (OA). **(a)** The thermodenuder was operated at 97–117 °C centerline temperature and about half of the total OA mass evaporated. The ambient OA spectrum (light green sticks, grey error bars) closely resembled the thermodenuded OA spectrum (orange dots, black error bars). Error bars are \pm the averaged errors calculated by the standard Q-AMS data analysis software (v1.41). **(b)** The average relative organic spectra when the thermodenuder was operated 140–150 °C centerline temperature and about 3/4 of the total OA mass evaporated. The spectra of the ambient and the thermodenuded OA are more distinct, but the differences are not statistically significant.

This is in contrast to observations in many laboratory experiments (Grieshop et al., 2009b) or in field studies closer to the sources (Huffman et al., 2009). In these studies, the thermodenuded organic aerosol is observed to have a larger f_{44} compared to the ambient aerosol. These observations are consistent with an inverse relationship between extent of oxidation and volatility: holding the carbon number of the molecule constant, more oxidized (functionalized) compounds have a lower volatility and are therefore more likely to remain in the aerosol phase upon heating. The OA sampled in these studies is a mixture of fresher and more oxidized OA, and the more oxidized OA is typically less volatile. Hence, the thermodenuded OA, from which the fresher, more volatile components have been stripped, exhibits higher f_{44} . During FAME-2008, however, almost all OA was highly oxidized, and the aged aerosol was not mixed with fresher OA (except possibly on 19–21 May as mentioned above). In this highly oxidized organic aerosol, f_{44} does not have an inverse relationship with volatility. The

lack of correlation between volatility and O:C is consistent with compounds produced via fragmentation or oligomerization. In the fragmentation pathway, O:C increases by net loss of carbon rather than net addition of oxygen (Kroll et al., 2009). Thus, an increase in O:C is not necessarily associated with a decrease in volatility since the decrease in volatility due to the addition of oxygen can be offset by an increase in volatility due to fragmentation. While fragmentation can result in compounds with different O:C but similar volatility, oligomerization can result in compounds of different volatility with similar O:C. The fragmentation pathway is more likely in highly oxidized organic aerosol; thus it may be the dominant pathway in the late stage of the oxidation process observed during FAME-2008. The available data do not allow us to more than speculate about the importance of this process.

3.2.3 Positive matrix factorization

Various PMF solutions (obtained with different numbers of factors, rotational states, etc.) were examined and evaluated with respect to mathematical diagnostics and ancillary data (not included in the PMF analysis, e.g. AMS-sulfate). The 2-factorial PMF solution (rotated by $f_{peak}=-0.20$) appears to best represent our data. For example, the sum of the squared, uncertainty-weighted residuals relative to its expected value (Q/Q_{exp}) decreased by 33% from the 1-factorial ($p=1$) to the 2-factorial ($p=2$) solution, but only by another 4% from $p=2$ to $p=3$. The unexplained mass fraction was about 1% using $p=1$, but $<0.1\%$ using $p=2$ and more factors. These and more details on the PMF analysis are discussed in Appendix C.

We first focus on the PMF results of the ambient data. The profiles of the two factors, both OOA-like, are presented in Fig. 8. We name the more oxidized factor OOA-1 ($f_{43}=4.5\%$, $f_{44}=21.7\%$) and the less oxidized factor OOA-2 ($f_{43}=6.5\%$, $f_{44}=13.1\%$), consistent with previous studies (Lanz et al., 2007; Morgan et al., 2010; Ulbrich et al., 2009). HOA (hydrocarbon-like organic aerosol) was not present in detectable amounts, as confirmed by several methods: unconstrained PMF (presented here), PMF with a prescribed/constrained HOA profile using the multilinear engine (Lanz et al., 2008), and correlations of f_{57} and HOA concentrations from Aiken et al. (2009) and Lanz et al. (2009). The absence of HOA in this dataset is different from most other published PMF data (Ng et al., 2010). This is consistent with the absence of sources close to the site and the very low measured f_{57} . The sources influencing the site surely contain primary as well as secondary organic aerosol, but when the aerosol reaches the site, it has been diluted and oxidized enough that all OA has been converted to OOA, a mixture of OPOA and SOA.

OOA-1 correlated with sulfate measured by the AMS ($R^2=0.68$), whereas OOA-2 did not ($R^2=0.00$). OOA-2 showed a weak correlation with AMS nitrate ($R^2=0.07$),

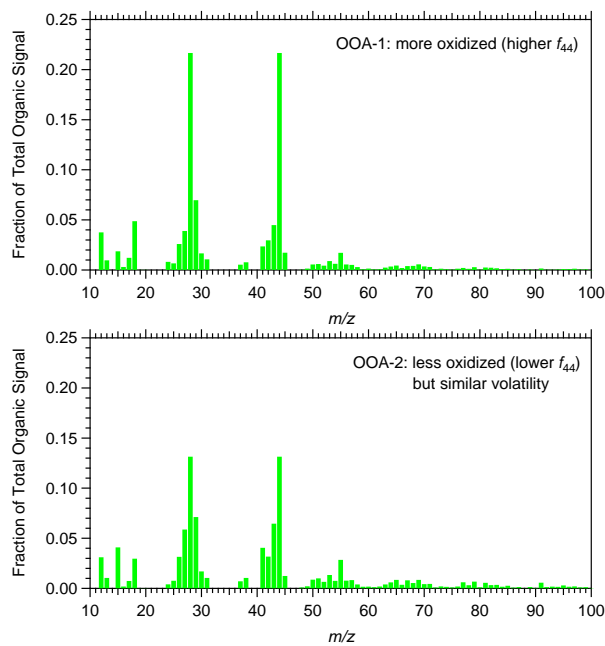


Fig. 8. Factor profiles of the more oxidized OOA-1 (top) and less oxidized OOA-2 (bottom).

while OOA-1 did not ($R^2=0.00$). Thus, OOA-1 was correlated with the less volatile inorganic component (sulfate). However, OOA-1 is not less volatile than OOA-2 according to the thermodenuder data: the factor profiles from PMF analysis on the full data set using ambient and thermodenuded OA (also referred to as TD-AMS-PMF, Huffman et al., 2009) are not significantly different from the factor profiles from PMF on the ambient data only (AMS-PMF). Furthermore, the contributions of the two factors are very similar in the full dataset (OOA-1 61%, OOA-2 39% on average) and in the ambient-only data set (59% and 41%, respectively). Figure 9 shows that, throughout the campaign, the relative fraction of OOA-1 in the total OA is the same in the ambient ($f_{OOA-1,bp}$) and the thermodenuded organic aerosol ($f_{OOA-1,TD}$). Orthogonal distance regression between $f_{OOA-1,bp}$ and $f_{OOA-1,TD}$ yields $R^2=0.79$, slope=1.01, and intercept=0.04. This is another indication that the organic aerosol measured during FAME-2008 does not exhibit the commonly observed inverse relationship between volatility and extent of oxidation, and it is the primary reason why we did not name the two OOA factors LV- and SV-OOA (Jimenez et al., 2009). In fact, the O:C₄₄ of OOA-1 and OOA-2 are approximately 0.9 and 0.6, respectively, and hence span the range of O:C previously associated with LV-OOA (Jimenez et al., 2009).

This raises the question of the physical meaning (other than differences in volatility) of the two OOA factors found here, and whether or not a 1-factor solution – yielding one OOA-component correlated with AMS-sulfate ($R^2=0.56$) –

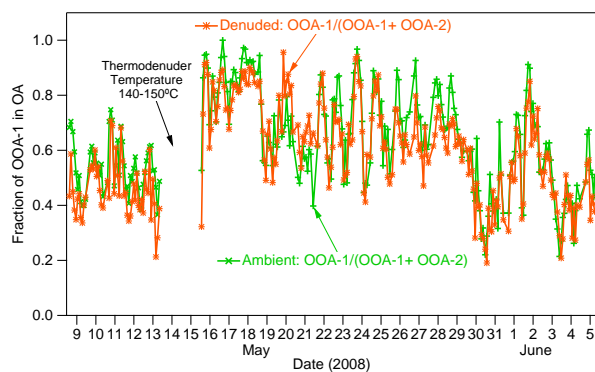


Fig. 9. The relative fractions of OOA-1 in the thermodenuded organic aerosol when the thermodenuder was operated at 97–117 °C centerline temperature (orange, stars) and of the ambient organic aerosol (green, crosses) are very similar throughout the campaign. The organic aerosol measured during FAME-2008 does not exhibit the expected inverse relationship between volatility and extent of oxidation.

might be more appropriate. Factor analysis is not always possible on highly aged organic aerosol datasets. For example, Dunlea et al. (2009) found that the limited spectral variability in their measured organic aerosol precluded them from separating it into physically meaningful factors. Here we explore the possible physical meanings of the two OOA factors found for FAME-2008. The physical meaning could, for example, be related to heterogeneous chemistry, photochemical aging and the aerosol source region. Considering that the organic aerosol observed at Finokalia was highly aged and exhibited low volatility (Lee et al., 2010), organic compounds may be mostly in the particle phase and additional aging may be primarily heterogeneous. Since the inorganic aerosol was usually acidic (Sect. 3.1, Fig. 10) heterogeneous chemistry may be even more favorable. If heterogeneous chemistry favors the production of one OOA component over the other, we expect inorganic acidity to correlate with the concentration of that OOA component. Figure 10 shows that there were some time periods during which the inorganic acidity of the particles correlated with the concentrations of OOA-1 and OOA-2 (e.g. 23–26 May, light green oval); however, this was not always the case (29–30 May, dark green oval). The overall correlation of, for example, the fraction of OOA-1 and acidity is very weak ($R^2=0.08$). This does, however, not rule out heterogeneous reactions, since Kalberer et al. (2004) showed that oligomerization proceeds also in the absence of inorganic acidity.

Another hypothesis is that the relative contribution of the two OOA factors is associated with OA aging and/or its source region. There are time periods during which the source and OH exposure of the OA appear to influence OOA concentrations. For example, Fig. 11 shows the time series of the OOA-2 plume during 29–30 May, when the aerosol

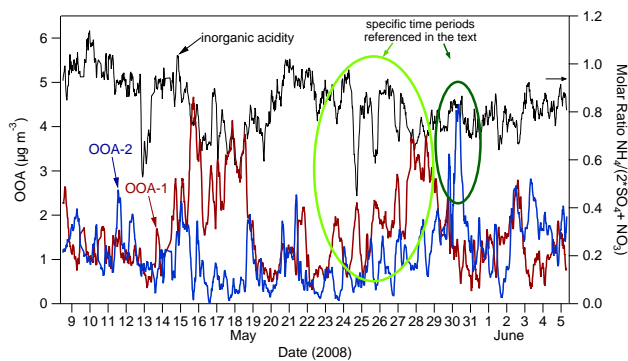


Fig. 10. Time series of PMF factors (OOA-1 and OOA-2, left vertical axis) and inorganic acidity (right vertical axis). During some time periods (23–26 May, light green oval), the concentrations of the factors are correlated with inorganic acidity. During other time periods (29–30 May, dark green oval), significant changes in the OOA factors are not accompanied by a significant change in inorganic acidity.

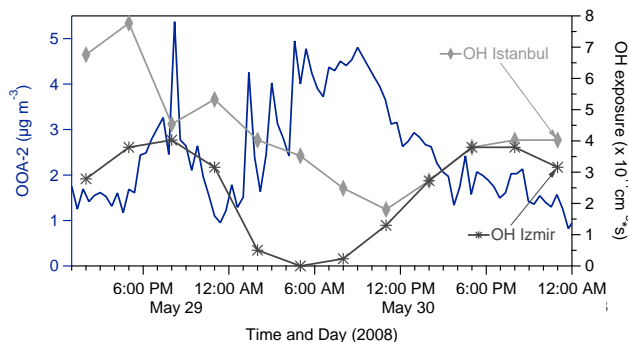


Fig. 11. Time series of OOA-2 (left vertical axis) on 29–30 May, when the air mass was influenced by Istanbul and Izmir, and the estimated OH exposures of the aerosol originating from these cities (right vertical axis). The concentration of OOA-2, the less oxidized organic aerosol, is negatively correlated with OH exposure, suggesting that OOA-2 concentrations are related to photochemical aging.

appeared to be influenced by Izmir and Istanbul, two major cities in Turkey. The figure also shows estimated OH exposures of the aerosol originating from these cities. During this time period, OH exposure is negatively correlated with the concentration of OOA-2, the fresher, less-oxidized organic aerosol. However, on average, the concentration of OOA-2 does not differ significantly across source regions (Sect. 3.3, Table 1). The presence of a diurnal cycle in OOA-1 and OOA-2 (Sect. 3.2.4) further suggests that changes in their concentrations are associated with atmospheric photo-oxidation. Thus, we propose that the OOA factors represent organic aerosol of different photochemical age and highlight that photochemical age here is not associated with a change in volatility, at least at this late stage in the oxidation process. The factors probably do not represent groups

Table 1. Source region analysis of organic aerosol: summary of results.

| Category (# points) | Marine (590) | Africa (134) | Athens (194) | Greece ^a (216) | Continental ^b (421) |
|--|-----------------|-----------------|-----------------|------------------------------|-----------------------------------|
| Organic Concentration ($\mu\text{g m}^{-3}$) | 2.1 ± 0.8^c | 1.9 ± 0.8 | 3.2 ± 0.9 | 2.6 ± 0.7 | 3.2 ± 1.0 |
| Sulfate ($\mu\text{g m}^{-3}$) | 3.0 ± 1.3 | 5.0 ± 1.7 | 7.5 ± 2.2 | 6.8 ± 3.0 | 5.9 ± 2.8 |
| f_{44} | 0.17 ± 0.02 | 0.19 ± 0.02 | 0.19 ± 0.015 | 0.20 ± 0.02 | 0.18 ± 0.02 |
| f_{43} | 0.05 ± 0.01 | 0.05 ± 0.01 | 0.05 ± 0.01 | 0.05 ± 0.01 | 0.05 ± 0.01 |
| OOA-1 ($\mu\text{g m}^{-3}$) | 1.0 ± 0.5 | 1.1 ± 0.5 | 2.1 ± 0.9 | 2.2 ± 0.9 | 1.9 ± 0.9 |
| OOA-2 ($\mu\text{g m}^{-3}$) | 1.2 ± 0.7 | 0.8 ± 0.6 | 1.2 ± 0.8 | 0.7 ± 0.5 | 1.5 ± 0.8 |

^a Air mass influenced by Greece but not Athens;

^b air mass continental, but not from Greece or Athens;

^c one standard deviation.

of organic compounds from separate sources but rather limits associated with continuous variation in organic composition due to chemical changes. While factor analysis can often be used to obtain insights into the sources of organic aerosol (e.g. Zhang et al., 2005b; Lanz et al., 2007, 2008), here it may be primarily useful by providing insights into chemical processes affecting OA composition.

3.2.4 Diurnal variation

Figure 12a shows the average diurnal variation of f_{43} and f_{44} . The aerosol becomes more oxidized (higher f_{44}) during the afternoon, when the photochemical activity is higher. The results of the ANOVA tests suggest that this diurnal variation is statistically significant for f_{44} ($p < 10^{-16}$) and f_{43} ($p = 2.2 \times 10^{-11}$). Harmonic analysis suggests that f_{43} has a diurnal cycle of amplitude 0.002 and a phase of -1.25 which can explain 77% of the variance, and f_{44} has a diurnal cycle of amplitude 0.007 and phase -1.50 , which can explain 73% of the variance. What is notable here is that the cycles of f_{43} and f_{44} have a similar phase: as f_{43} decreases, f_{44} increases. This may partly be caused by functional groups leading to m/z 43 fragments being oxidized to functional groups leading to m/z 44 fragments. OOA-1 and OOA-2 also have statistically significant diurnal cycles (Fig. 12b). The OOA-1 diurnal cycle ($p = 1.4 \times 10^{-12}$) has phase -1.54 , amplitude $0.31 \mu\text{g m}^{-3}$ and can explain 81% of the variance. The OOA-2 diurnal cycle ($p = 5.5 \times 10^{-8}$) has phase 1.17, amplitude $0.20 \mu\text{g m}^{-3}$ and can explain 65% of the variance. Thus, the OOA-1 diurnal cycle has a very similar phase as the f_{44} diurnal cycle, and the OOA-2 diurnal cycle has a similar phase as the f_{43} diurnal cycle. This may indicate that the OOA-1 factor is driven by f_{44} and the OOA-2 factor is driven by f_{43} .

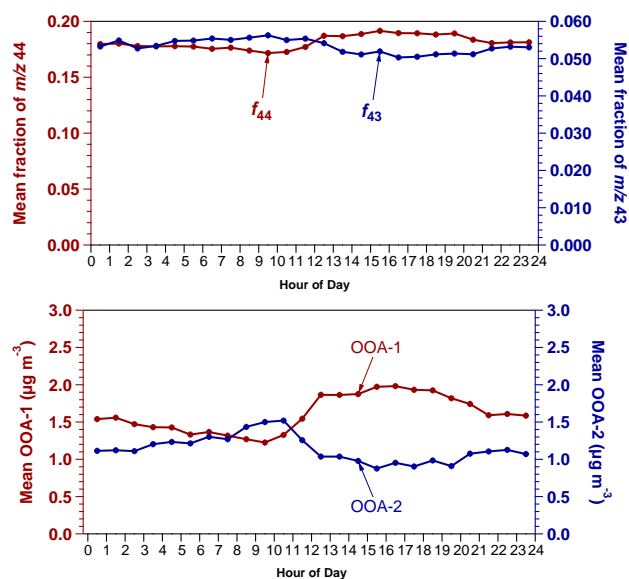


Fig. 12. (a) Diurnal trend of f_{44} (left vertical axis, amplitude=0.007, phase= -1.50 , $p < 10^{-16}$) and f_{43} (right vertical axis, amplitude=0.002, phase= -1.25 , $p = 2.2 \times 10^{-11}$). (b) Diurnal trend of OOA-1 (left vertical axis, amplitude= $0.31 \mu\text{g m}^{-3}$, phase= -1.55 , $p = 1.4 \times 10^{-12}$) and OOA-2 (right vertical axis, amplitude= $0.20 \mu\text{g m}^{-3}$, phase= -1.16 , $p = 2.2 \times 10^{-11}$). The presence of diurnal trends provides evidence for photochemical aging.

With photochemical aging, the organic aerosol evolves from a less oxidized to a more highly oxidized state. The amplitude of the diurnal cycles is small, presumably because the local aging is slow (Sect. 3.2.1) and most of the aging has happened before the particles approach the site. Diurnal cycles in the OA composition are consistent with the notion

of ongoing oxidation at the site. The lack of a diurnal cycle in the total OA concentration, despite the diurnal cycle in its composition, is consistent with the lack of correlation between extent of oxidation and volatility (Sect. 3.2.2).

3.3 Analysis by source region

Table 1 presents the means and standard deviations of bulk sulfate and organic concentrations, f_{44} , f_{43} , OOA-1, and OOA-2 for the aerosol from different source regions sampled during the campaign. The source region analyses of additional species, as well as a figure indicating the source region of the aerosol sampled at any time during the campaign, is presented in our companion paper (Pikridas et al., 2010). Total OA concentrations exhibit little variation with source region, suggesting mostly regional sources of the organic species. In contrast, sulfate concentrations exhibit more variation with source region, consistent with point sources in Greece and the Balkans as the source of most sulfate sampled at Finokalia. The extent of oxidation of the OA, indicated by f_{44} , does not vary significantly by source region. Interestingly, aerosol that appears to be influenced by Athens or the rest of Greece, the two closest continental source regions, does not exhibit a lower f_{44} than aerosol from the other source regions. By the time it reaches the measurement site, the OA has been diluted and aged enough that it is indistinguishable from the other continental aerosol. The fraction of organic aerosol mass at m/z 43, f_{43} , does not vary by source region at all. OOA-1 does vary with source region, exhibiting higher concentrations when the air mass originated from more polluted areas. OOA-2, however, does not show a clear trend with source region. One might expect that OOA-2, if it is the “fresher” (less oxidized) organic aerosol, would be higher from the more polluted regions. The more oxidized organic aerosol, OOA-1, is expected to be more regional and therefore more constant with source region. Instead, we observe that OOA-1 is variable and higher from the more polluted source regions. We hypothesize that causes other than time, for example oxidant concentrations, drive the difference in the “aging” of organic aerosol. For example, if polluted air masses contain significant amounts of ozone, the availability of water (from the sea) and sunlight may produce high oxidant concentrations (OH and O₃) in those air masses, resulting in more oxidized organic aerosol. Categorization into even more source regions provided no additional insights about the OA (Pikridas et al., 2010).

4 Conclusions

The NR-PM₁ sampled during FAME-2008 was mostly composed of inorganic species, and the organic fraction, which accounted for about 28% of the dry NR-PM₁, was highly oxidized. The aerosol sampled originated in pristine (e.g. marine) and polluted regions (e.g. Athens). Oxidizing con-

ditions observed during FAME-2008 were strong, resulting in similar composition and concentration of organic aerosol regardless of the source region. Organic aerosol composition followed a small but significant diurnal cycle, suggesting that atmospheric photo-oxidation at the site was ongoing but slow. The organic mass spectrum did not change appreciably upon heating and evaporating about half of its mass in a thermodenuder. One potential explanation is that the compounds that remain in the particulate phase in this remote area had very similar AMS spectra and/or volatilities.

Factor analysis of the organic aerosol resulted in two components, both resembling oxygenated organic aerosol (OOA). Hydrocarbon-like organic aerosol (HOA) was not present in detectable amounts. The two OOA factors differ in extent of oxidation but not in volatility; both factors fall into the low-volatility OOA range. Organic aerosol factors obtained from factor analysis often arise from distinct air masses or sources, but this does not appear to be the case here. Instead, the factors appear to represent limits in a relatively continuous chemical variation arising from different levels of aging.

Atmospheric oxidation appears to converge to a highly oxidized organic aerosol, regardless of the original organic aerosol source – be it primary or secondary. This implies that the oxidation state, which can be approximated as a function of f_{44} , can be used to map the atmospheric evolution of organic aerosol.

Appendix A

AMS calibration and data work-up

A1 Details on AMS calibrations

The ionization efficiency (IE) of the AMS was measured every few days (six times between 9 May and 5 June, the time period in which AMS data was acquired) using dried ammonium nitrate particles with a diameter of 300 or 350 nm. The ratio of IE to the MS airbeam (AB) was constant for these calibrations (within noise), so the average IE/AB value of $4.18 \times 10^{-13} \text{ Hz}^{-1}$ was used for the whole campaign, and the IE was determined at any point by multiplying IE/AB by the current AB. The relative ionization efficiency (RIE) of ammonium measured during the IE calibrations ranged from 4.16 to 4.58. The variation in the values appeared random; therefore the average value of 4.38 was used for the entire campaign. This is different from the standard value of 4.0. The flow rate in the AMS was $2.5 \text{ cm}^3 \text{ s}^{-1}$. Lens alignment, flow calibration and size calibration were performed at the beginning of the campaign.

A2 Adjustments to standard fragmentation table

A2.1 Air fragmentation

The fragmentation pattern of air at m/z 44 (CO_2^+), m/z 29 (N^{15}N^+) and m/z 16 (O^+) was evaluated using difference spectra (signal – background) during filter measurements. Filter measurements were taken at various times during the campaign before and after every change in the instrument (e.g. ionization efficiency calibration). There were 11 filter periods (corresponding to a total of 3.5 h of filter data) used for the adjustment of the air fragmentation pattern. N^{15}N^+ and CO_2^+ were calculated as constant fractions of the N_2^+ signal at m/z 28. The calculated fraction of N^{15}N^+ ranged from 0.00722–0.00723, slightly different from the standard value of 0.00736. O^+ was calculated as a constant fraction of N^+ . The calculated ratio ranged from 0.305 to 0.330, different from the standard value of 0.353. The calculated fraction of CO_2^+ ranged from 0.000826 to 0.000884, different from the standard value of 0.000734. The ratio m/z 44: m/z 28 is not simply the CO_2 mixing ratio in the air but also accounts for ion transmission differences, the relative ionization efficiency of CO_2 , and a correction for the m/z 14 fragmentation of nitrogen. Therefore, a coefficient deviating from the standard coefficient does not necessarily imply a difference in the CO_2 mixing ratio but may be due to differences in the other factors, which can vary between instruments.

A2.2 Organic fragmentation

Based on the recommendation by Aiken et al. (2008), we used the following fragmentation pattern in relation to the m/z 44 signal: m/z 28=100%, m/z 18=22.5%. In the original AMS fragmentation table, these were set to 0% and 100% respectively.

A2.3 Water fragmentation

Water dominates the signal in the background (closed) spectrum at m/z 16 (O^+) m/z 17 (OH^+) and m/z 18 (H_2O^+). The water fragmentation pattern can be determined by plotting the closed signal of m/z 16 vs. m/z 18 and m/z 17 vs. m/z 18. In this way, we determined that O^+ =4% of H_2O^+ (as in the standard fragmentation table) and OH^+ =27.6% of H_2O^+ (slightly different from the 25% in the standard fragmentation table).

A2.4 Correction for gas-phase water (absolute humidity)

In the AMS data analysis software, the particle water signal is determined by subtracting the water vapor signal from the total water signal. By default, the water vapor signal at m/z 18 (H_2O^+) is set to 1% of the N_2^+ signal at m/z 28. The actual water vapor signal (relative to N_2^+) varies with ambient humidity.

There are two ways to adjust the AMS data based on ambient humidity: 1) using the measurements during the filter periods, and 2) using the particle time-of-flight data of m/z 18 and m/z 28. The fundamental assumption made in both corrections is that the ratio of $\text{H}_2\text{O}^+(\text{vapor})/\text{N}_2^+$ measured by the AMS scales with the absolute humidity.

Water correction using filter periods

In the following, let w_ratio be the mass ratio of water vapor to N_2 in the air: $w_ratio=\text{H}_2\text{O}^+(\text{vapor})/\text{N}_2^+$. Then, abbreviating the absolute humidity as AH , the relationship between w_ratio at two different absolute humidities AH_1 and AH_2 is given by:

$$\frac{w_ratio_1}{w_ratio_2} = \frac{\text{AH}_1}{\text{AH}_2} \quad (\text{A1})$$

or

$$w_ratio_2 = \frac{w_ratio_1}{\text{AH}_1} \cdot \text{AH}_2 \quad (\text{A2})$$

If w_ratio and absolute humidity are both known at a particular time during the campaign, and if measurements of the ambient absolute humidity are available throughout the campaign, the time-dependent w_ratio can be determined for the duration of the campaign:

$$w_ratio(t) = \frac{w_ratio_{\text{ref}}}{\text{AH}_{\text{ref}}} \cdot \text{AH}(t) \quad (\text{A3})$$

We calculated the absolute humidity throughout the campaign using the following steps:

- 1) Calculating the saturation partial vapor pressure of H_2O using the measured ambient temperature.
- 2) Calculating the saturation water mixing ratio (by mass) using the saturation partial vapor pressure of H_2O and ambient pressure.
- 3) Calculating the absolute humidity, i.e. the water mixing ratio (by mass) using the saturation water mixing ratio (by mass) and the measured ambient relative humidity.

As reference values for w_ratio and AH we used data during the filter periods when only gases are measured and all water signal is due to water vapor.

Water correction using the particle time-of-flight data

In the particle time-of-flight (pToF) spectra, gas-phase species occur earlier in the pToF spectrum than particle-phase species. It is therefore possible to separate gas-phase and particle-phase signal in pToF. The advantage of this procedure is that all of the data – not just the data during the filter periods – can be used.

The procedure is to integrate the m/z 18 and the m/z 28 pToF signals in the gas-phase only. w_ratio is then given by the ratio of these two integrals.

It is not possible to do this analysis for every time step due to the noise in the pToF spectra. Therefore, we binned all AMS data by ambient absolute humidity (0.04–0.13), averaged the m/z 18 and m/z 28 spectra for the different bins, integrated them and calculated w_{ratio} . We then computed the linear fit between w_{ratio} and AH, and we used the resulting function to compute w_{ratio} at all times (and at all AH) during the campaign.

For the ambient data, the two water corrections (using filter data or using pToF data) yielded very similar results. For the thermodenuded data, the results were also similar. But, the pToF correction yielded more physical data as it resulted in fewer time periods of water concentrations less than zero in the thermodenuded aerosol. We therefore used the pToF water correction for all of the data.

Appendix B

Estimating OH exposure corresponding to 1 day of atmospheric aging during FAME-2008

We used values of j_{NO_2} measured during FAME-2008 and correlations developed by Berresheim et al. (2003) to first approximate $j_{\text{O}^1\text{D}}$ (the photolysis rate of O^1D) from j_{NO_2} (Berresheim et al., 2003, Fig 4) and then $[\text{OH}]$ from $j_{\text{O}^1\text{D}}$ (Berresheim et al., 2003, Fig. 6). As expected, during FAME-2008 j_{NO_2} was highest between 12:00–13:00 local standard time: mean $8.0 \times 10^{-3} \text{ s}^{-1}$, interquartile range $8.0\text{--}8.4 \times 10^{-3} \text{ s}^{-1}$. Using the correlations, the mean value of $8.0 \times 10^{-3} \text{ s}^{-1}$ corresponds to an approximate $[\text{OH}]$ of $1.5 \times 10^7 \text{ cm}^{-3}$. Assuming that the daily trend of $[\text{OH}]$ is sinusoidal (Russell et al., 1994), we model $[\text{OH}]$ as a sine wave that is zero at 06:00 and at 19:00 and reaches its maximum of $1.5 \times 10^7 \text{ cm}^{-3}$ at 12:30. By integrating this sine wave, we obtain an approximate OH exposure of $4.4 \times 10^{11} \text{ molecules cm}^{-3} \text{ s}$ for one day of aging during FAME-2008.

Appendix C

C1 General remarks

Different PMF solutions can be obtained by varying the PMF settings, model parameters, and the input matrix, \mathbf{X} . Several PMF settings and their influence on the factor time series, \mathbf{G} , factor profiles, \mathbf{F} , as well as (uncertainty-scaled) residuals, \mathbf{Q} and \mathbf{E} , of the organic aerosol (OA) data from Finakolia were explored. This includes the choice of different subsets of organic m/z 's in the PMF data matrix \mathbf{X} (m/z 's 12...300 vs. m/z 's 12...100), specifying different "error models" (e.g., adding modeling uncertainty to the instrumental uncertainty), using different pseudo-random starting values for the algorithm in PMF2 (i.e., changing the "seed"-numbers), excluding OA

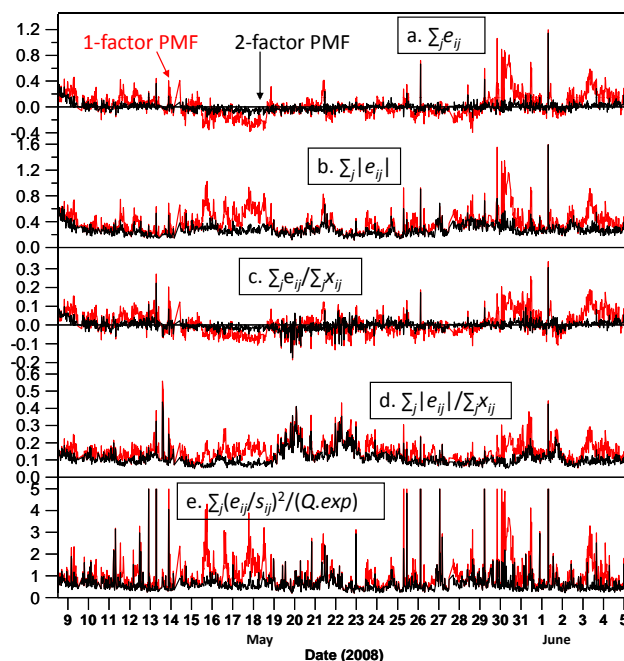


Fig. C1. Model residuals, $E = X - GF$, for the 1-factor (red lines) and the 2-factor (black lines) PMF solutions as a function of time (summed over all m/z 's) calculated in five different ways: a. sum of $E(t)$, b. sum of $|E(t)|$, c. sum of $E(t)$ relative to total organics, d. sum of $|E(t)|$ relative to total organics, and e. sum of squared, uncertainty-weighted ("scaled") residuals, $Q(t) = E(t)/S(t)$, relative to expected values, $Q \cdot \exp(t)$. Plots obtained with the PMF evaluation tool, PET, by Ulbrich et al. (2009). The structure in the residuals is decreased significantly in the $p=2$ solution compared to the $p=1$ solution.

plumes from the data matrix \mathbf{X} , using different averaging times, or different convergence criteria.

Here we use two criteria to evaluate the stability of the PMF solution with respect to these choices: 1) The percent change in f_{43} and f_{44} between the base case (base) and the modified case (mod): $[f_{43,44}(\text{base}) - f_{43,44}(\text{mod})]/f_{43,44}(\text{mod})$, and 2) the slope, intercept and R^2 of the orthogonal distance regressions between factors obtained via the base case and the modified cases. The PMF solutions were found to be quite stable with respect to the settings and inputs mentioned above. For example, a 3% increase in the modeling uncertainty changed $f_{43,44}$ by less than 3%. The orthogonal distance regression between the base case and this modified case yielded slope=0.93, intercept=0.06 $\mu\text{g m}^{-3}$, $R^2=0.99$ for OOA-1 and slope=0.96, intercept=0.11 $\mu\text{g m}^{-3}$, $R^2=0.98$ for OOA-2. Changing the other settings had an even smaller effect than changing the modeling uncertainty.

In contrast, choosing different numbers of factors, p , and inducing rotations by the "fpeak"-parameter exerted a comparatively strong influence on the PMF solutions. For example, varying f_{peak} between 0.00...−0.20 changed $f_{43,44}$

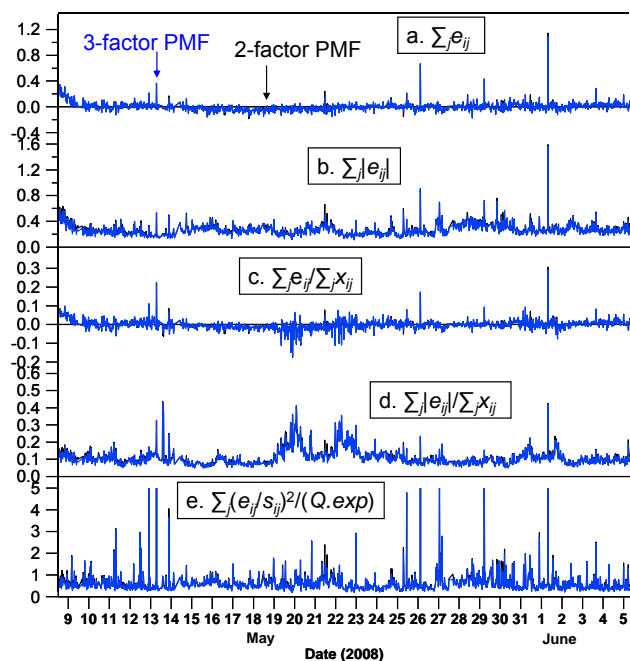


Fig. C2. Model residuals, $E=X-GF$, for the 2-factor (black lines) and the 3-factor (blue lines) PMF solutions as a function of time (summed over all m/z 's) calculated in five different ways: a. sum of $E(t)$, b. sum of $|E(t)|$, c. sum of $E(t)$ relative to total organics, d. sum of $|E(t)|$ relative to total organics, and e. the sum of squared, uncertainty-weighted (“scaled”) residuals, $Q(t) = E(t)/S(t)$, relative to expected values, $Q \cdot \exp(t)$. Plots obtained with the PMF evaluation tool, PET, by Ulbrich et al. (2009). The structure in the residuals was not reduced notably from the $p=2$ to the $p=3$ solution.

by as much as 30%. Therefore, the roles of the number of PMF factors as well as the rotational state of the solutions are discussed in the following sections. The presented solutions were obtained from the complete data matrix \mathbf{X} (organic m/z 12...300, including OA plumes), averaged to 9-min resolution using PMF default settings (robust mode= T , outlier threshold=4, modeling uncertainty=0%). The consecutive PMF runs and the visualization of the PMF output were mediated via the PMF evaluation tool, PET, described by Ulbrich et al. (2009).

C2 Number of factors (p)

First, we investigated the choice of different numbers of factors, p , with respect to ancillary data. The 1-factorial PMF solution yielded a spectrum resembling OOA, and the corresponding time series correlated with particulate sulfate (measured with the Q-AMS) at $R^2=0.56$. However, the correlation with AMS-sulfate was even higher ($R^2=0.68$) for OOA-1 obtained by the 2-factor PMF. In addition, the second factor OOA-2 coincided episodically (was weakly correlated) with AMS-nitrate. The solutions for $p=3$ and more factors resulted in at least two time series that were highly corre-

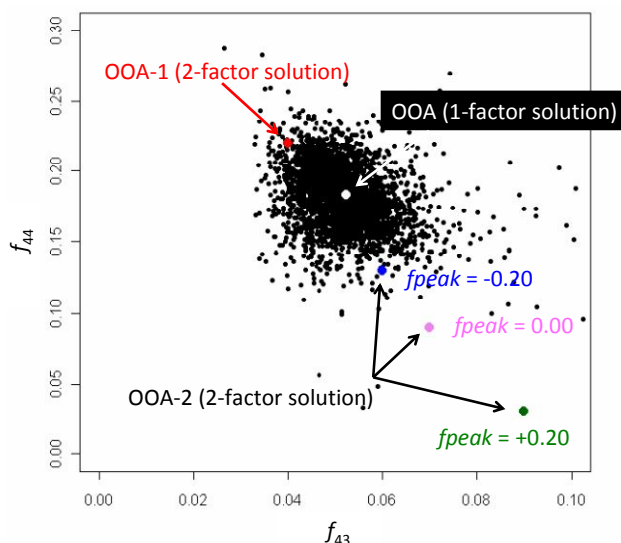


Fig. C3. Organic aerosol data represented as black dots in the plane f_{43} (horizontal axis) vs. f_{44} (vertical axis). The colored dots represent the position of calculated PMF-factors: OOA-1 at $f_{peak}=-0.20$, 0.00, +0.20 (red), OOA-2 at $f_{peak}=-0.20$ (blue), 0.00 (violet), +0.20 (green), and OOA (as retrieved by the 1-factor solution) in white. The variation of OOA-1 with f_{peak} was not detectable; hence the values appear as one dot.

lated and spectra indicative of splitting artifacts (e.g., OOA split into two spectra exhibiting preeminent contributions of m/z 44 and m/z 29, respectively).

Second, we evaluated mathematical diagnostics. The sum of the squared, uncertainty-weighted residuals relative to its expected values Q/Q_{exp} , was close to 1 or lower for $p=1...3$. This ratio decreased by 33% from $p=1$ to $p=2$, but only by another 4% from $p=2$ to $p=3$ (representing a comparatively low decrease). At $p=2$, Q/Q_{exp} increased by only +0.01% from $f_{peak}=0.0$ to $f_{peak}=-0.2$. The unexplained mass fraction was about 1% using $p=1$, but <0.1% using $p=2$ and more factors.

Moreover, we analyzed the model residuals, \mathbf{E} , as a function of time. Structures in these residuals indicate that some OA processes and/or OA sources cannot be fully approximated by the model. The structure in the model residuals could be markedly reduced by increasing the number of factors from $p=1$ to $p=2$ (Fig. C1). When further increasing the number of factors from $p=2$ to $p=3$ only a minor decrease of the model residuals, \mathbf{E} , could be observed (Fig. C2).

C3 Inducing different rotational states (f_{peak})

Based on considerations presented in Sect. C2 and in the manuscript, we focus on the 2-factor PMF solution and examine rotations for that solution here. Roughly speaking, $f_{peak}<0$, $f_{peak}>0$, and $f_{peak}=0$ discriminate three different PMF-AMS cases similar with respect to the shape of OOA-1,

and the time trends of both OOA-1 and OOA-2 (and the corresponding pattern of the daily cycles). However, these cases are quite different in the relative peak intensities of organic masses at m/z 43 and m/z 44, f_{43} and f_{44} , particularly in OOA-2 (where $f_{43} < f_{44}$ if $f_{peak} < 0$, $f_{43} \approx f_{44}$ if $f_{peak} = 0$, and $f_{43} > f_{44}$ if $f_{peak} > 0$; cf. Fig. C3), and also with respect to the relative abundances [%OA] of OOA-1 and OOA-2. The relative OOA-1 fraction is 55%...61% for $f_{peak} = -1.00$... -0.05 , it is 72% for $f_{peak} = 0$, and it is 79%...81% for $f_{peak} = +0.05$... $+1.00$.

There are three reasons for choosing a negative f_{peak} (and/or specifically an $f_{peak} = -0.20$). First, with increasing values of f_{peak} , low S/N (signal-to-noise) fragments become more increasingly important, e.g., for $f_{peak} > 0$, f_{15} has similar magnitude as f_{43} or f_{44} . In other words, with increasing f_{peak} -values the PMF factor profiles become dissimilar from realistic OA components (also represented in Fig. C3). Second, the TD-AMS-PMF (i.e., data matrix \mathbf{X}' included ambient and thermodenuded OA data) results are relatively similar to AMS-PMF (i.e., data matrix, \mathbf{X} , included ambient OA data exclusively) at $f_{peak} = -0.20$, which is consistent with the relative organic spectra measured by the AMS: the spectrum of the ambient organic aerosol is indistinguishable from the spectrum of the thermodenuded organic aerosol (Fig. 8 in the manuscript). Third, the profile at $f_{peak} = -0.20$ might be more “realistic” than the one at higher f_{peak} . Explicitly, the OOA-2 – profile at $f_{peak} = -0.20$ is closer to the typical data, which is represented by the plane f_{43} vs. f_{44} in Fig. C3, than it would be the case for $f_{peak} > -0.20$. This projection of the data further shows that OOA-2 (at $f_{peak} = -0.20$) and OOA-1 span the continuum of OA with respect to observed f_{43}/f_{44} -ratios (discarding some outliers), and the 1-factor OOA can be viewed as a centered solution.

Acknowledgements. This research was supported by the US National Science Foundation (ATM-0336296), the FP6 project EUCAARI – European Integrated Project on Aerosol Cloud Climate and Air Quality Interactions, as well as the Competence Center Environment and Sustainability of the ETH Domain (CCES) project IMBALANCE – Impact of Biomass Burning Aerosol on Air Quality and Climate. Travel support was provided by the FP6 project ACCENT – Atmospheric Composition Change – the European Network of Excellence. Lea Hildebrandt was supported by a National Science Foundation Graduate Research Fellowship.

Edited by: V.-M. Kerminen

References

- Aiken, A. C., DeCarlo, P. F., Kroll, J. H., Worsnop, D. R., Huffman, J. A., Docherty, K., Ulbrich, I. M., Mohr, C., Kimmel, J. R., Sueper, D., Sun, Y., Zhang, Q., Trimborn, A. M., Northway, M. J., Ziemann, P. J., Canagaratna, M. R., Alfarra, M. R., Prevot, A. S. H., J., D., Duplissy, J., Metzger, A., Baltensperger, U., and Jimenez, J. L.: O/C and OM/OC ratios of primary, secondary, and ambient organic aerosols with high resolution time-

of-flight aerosol mass spectrometry, *Environ. Sci. Technol.*, 42, 4478–4485, 2008.

Aiken, A. C., Salcedo, D., Cubison, M. J., Huffman, J. A., DeCarlo, P. F., Ulbrich, I. M., Docherty, K. S., Sueper, D., Kimmel, J. R., Worsnop, D. R., Trimborn, A., Northway, M., Stone, E. A., Schauer, J. J., Volkamer, R. M., Fortner, E., de Foy, B., Wang, J., Laskin, A., Shutthanandan, V., Zheng, J., Zhang, R., Gaffney, J., Marley, N. A., Paredes-Miranda, G., Arnott, W. P., Molina, L. T., Sosa, G., and Jimenez, J. L.: Mexico City aerosol analysis during MILAGRO using high resolution aerosol mass spectrometry at the urban supersite (T0) – Part 1: Fine particle composition and organic source apportionment, *Atmos. Chem. Phys.*, 9, 6633–6653, 2009, <http://www.atmos-chem-phys.net/9/6633/2009/>.

Allan, J. D., Jimenez, J. L., Williams, P. I., Alfarra, M. R., Bower, K. N., Jayne, J. T., Coe, H., and Worsnop, D. R.: Quantitative sampling using an Aerodyne aerosol mass spectrometer – 1. Techniques of data interpretation and error analysis, *J. Geophys. Res.-Atmos.*, 108(D3), 4090, doi:10.1029/2002JD002358, 2003., 2003.

Allan, J. D., Delia, A. E., Coe, H., Bower, K. N., Alfarra, M. R., Jimenez, J. L., Middlebrook, A. M., Drewnick, F., Onasch, T. B., Canagaratna, M. R., Jayne, J. T., and Worsnop, D. R.: A generalised method for the extraction of chemically resolved mass spectra from aerodyne aerosol mass spectrometer data, *J. Aerosol Sci.*, 35, 909–922, 2004.

An, W. J., Pathak, R. K., Lee, B.-H., and Pandis, S. N.: Aerosol volatility measurement using an improved thermodenuder: Application to secondary organic aerosol, *J. Aerosol Sci.*, 38, 305–314, 2007.

Atkinson-Palombo, C. M., Miller, J. A., and Balling Jr., R. C.: Quantifying the ozone “weekend effect” at various locations in Phoenix, Arizona, *Atmos. Environ.*, 40, 7644–7658, 2006.

Bahreini, R., Ervens, B., Middlebrook, A. M., Warneke, C., de Gouw, J. A., DeCarlo, P. F., Jimenez, J. L., Brock, C. A., Neuman, J. A., Ryerson, T. B., Stark, H., Atlas, E., Brioude, J., Fried, A., Holloway, J. S., Peischl, J., Richter, D., Walega, J., Weibring, P., Wollny, A. G., and Fehsenfeld, F. C.: Organic aerosol formation in urban and industrial plumes near Houston and Dallas, Texas, *J. Geophys. Res.-Atmos.*, 114, D00F16, doi:10.1029/2008JD011493, 2009.

Berresheim, H., Plass-Dülmer, C., Elste, T., Mihalopoulos, N., and Rohrer, F.: OH in the coastal boundary layer of Crete during MINOS: Measurements and relationship with ozone photolysis, *Atmos. Chem. Phys.*, 3, 639–649, 2003, <http://www.atmos-chem-phys.net/3/639/2003/>.

Bukowiecki, N., Lienemann, P., Hill, M., Figi, R., Richard, A., Furger, M., Rickers, K., Falkenberg, G., Zhao, Y., Cliff, S., Baltensperger, U., and Gehrig, R.: Real-world emission factors for antimony and other brake wear related trace elements: size-segregated values for light and heavy duty vehicles, *Environ. Sci. Technol.*, 43, 8072–8078, doi:10.1021/es9006096, 2009.

Canagaratna, M. R., Jayne, J. T., Jimenez, J. L., Allan, J. D., Alfarra, M. R., Zhang, Q., Onasch, T. B., Drewnick, F., Coe, H., Middlebrook, A. M., Delia, A., Williams, L. R., Trimborn, A. M., Northway, M. J., DeCarlo, P. F., Kolb, C. E., Davidovits, P., and Worsnop, D. R.: Chemical and microphysical characterization of ambient aerosols with the Aerodyne aerosol mass spectrometer, *Mass Spectrom. Rev.*, 26, 185–222, 2007.

- Chan, A. W. H., Kautzman, K. E., Chhabra, P. S., Surratt, J. D., Chan, M. N., Crouse, J. D., Krten, A., Wennberg, P. O., Flagan, R. C., and Seinfeld, J. H.: Secondary organic aerosol formation from photooxidation of naphthalene and alkylnaphthalenes: implications for oxidation of intermediate volatility organic compounds (IVOCs), *Atmos. Chem. Phys.*, 9, 3049–3060, 2009, <http://www.atmos-chem-phys.net/9/3049/2009/>.
- Capes, G., Johnson, B., McFiggans, G., Williams, P. I., Haywood, J., and Coe, H.: Aging of biomass burning aerosols over West Africa: aircraft measurements of chemical composition, microphysical properties, and emission ratios, *J. Geophys. Res.-Atmos.*, 113, D00C15, doi:10.1029/2008JD009845, 2008.
- Davidson, C. I., Phalen, R. F., and Solomon, P. A.: Airborne particulate matter and human health: A review, *Aerosol Sci. Tech.*, 39, 737–749, 2005.
- DeCarlo, P. F., Kimmel, J. R., Trimborn, A. M., Northway, M. J., Jayne, J. T., Aiken, A. C., Gonin, M., Fuhrer, K., Horvath, T., Docherty, K. S., Worsnop, D. R., and Jimenez, J. L.: Field-deployable, High-Resolution, Time-of-Flight Aerosol Mass Spectrometer, *Anal. Chem.*, 78, 8281–8289, 2006.
- DeCarlo, P. F., Dunlea, E. J., Kimmel, J. R., Aiken, A. C., Sueper, D., Crouse, J., Wennberg, P. O., Emmons, L., Shinozuka, Y., Clarke, A., Zhou, J., Tomlinson, J., Collins, D. R., Knapp, D., Weinheimer, A. J., Montzka, D. D., Campos, T., and Jimenez, J. L.: Fast airborne aerosol size and chemistry measurements above Mexico City and Central Mexico during the MILAGRO campaign, *Atmos. Chem. Phys.*, 8, 4027–4048, 2008, <http://www.atmos-chem-phys.net/8/4027/2008/>.
- Dockery, D. W., Pope, C. A., Xu, X. P., Spengler, J. D., Ware, J. H., Fay, M. E., Ferris, B. G., and Speizer, F. E.: An association between air-pollution and mortality in 6 United-States cities, *New Engl. J. Med.*, 329, 1753–1759, 1993.
- Donahue, N. M., Robinson, A. L., and Pandis, S. N.: Atmospheric organic particulate matter: From smoke to secondary organic aerosol, *Atmos. Environ.*, 43, 94–106, 2009.
- Dunlea, E. J., DeCarlo, P. F., Aiken, A. C., Kimmel, J. R., Peltier, R. E., Weber, R. J., Tomlinson, J., Collins, D. R., Shinozuka, Y., McNaughton, C. S., Howell, S. G., Clarke, A. D., Emmons, L. K., Apel, E. C., Pfister, G. G., van Donkelaar, A., Martin, R. V., Millet, D. B., Heald, C. L., and Jimenez, J. L.: Evolution of Asian aerosols during transpacific transport in INTEX-B, *Atmos. Chem. Phys.*, 9, 7257–7287, 2009, <http://www.atmos-chem-phys.net/9/7257/2009/>.
- Goldstein, A. H. and Galbally, I. E.: Known and unexplored organic constituents in the Earth's atmosphere, *Environ. Sci. Technol.*, 41, 1515–1521, 2007.
- Grieshop, A. P., Logue, J. M., Donahue, N. M., and Robinson, A. L.: Laboratory investigation of photochemical oxidation of organic aerosol from wood fires 1: measurement and simulation of organic aerosol evolution, *Atmos. Chem. Phys.*, 9, 1263–1277, 2009a, <http://www.atmos-chem-phys.net/9/1263/2009/>.
- Grieshop, A. P., Donahue, N. M., and Robinson, A. L.: Laboratory investigation of photochemical oxidation of organic aerosol from wood fires 2: analysis of aerosol mass spectrometer data, *Atmos. Chem. Phys.*, 9, 2227–2240, 2009b, <http://www.atmos-chem-phys.net/9/2227/2009/>.
- Hallquist, M., Wenger, J. C., Baltensperger, U., Rudich, Y., Simpson, D., Claeys, M., Dommen, J., Donahue, N. M., George, C., Goldstein, A. H., Hamilton, J. F., Herrmann, H., Hoffmann, T., Iinuma, Y., Jang, M., Jenkin, M. E., Jimenez, J. L., Kiendler-Scharr, A., Maenhaut, W., McFiggans, G., Mentel, Th. F., Monod, A., Prévôt, A. S. H., Seinfeld, J. H., Surratt, J. D., Szmigielski, R., and Wildt, J.: The formation, properties and impact of secondary organic aerosol: current and emerging issues, *Atmos. Chem. Phys.*, 9, 5155–5236, 2009, <http://www.atmos-chem-phys.net/9/5155/2009/>.
- Hildebrandt, L., Donahue, N. M., and Pandis, S. N.: High formation of secondary organic aerosol from the photo-oxidation of toluene, *Atmos. Chem. Phys.*, 9, 2973–2986, 2009, <http://www.atmos-chem-phys.net/9/2973/2009/>.
- Huffman, J. A., Docherty, K. S., Aiken, A. C., Cubison, M. J., Ulbrich, I. M., DeCarlo, P. F., Sueper, D., Jayne, J. T., Worsnop, D. R., Ziemann, P. J., and Jimenez, J. L.: Chemically-resolved aerosol volatility measurements from two megacity field studies, *Atmos. Chem. Phys.*, 9, 7161–7182, 2009, <http://www.atmos-chem-phys.net/9/7161/2009/>.
- IPCC: Climate Change 2007 – The Physical Science Basis, Contribution of working group I to the fourth assessment report of the IPCC, 2007.
- Jayne, J. T., Leard, D. C., Zhang, X. F., Davidovits, P., Smith, K. A., Kolb, C. E., and Worsnop, D. R.: Development of an aerosol mass spectrometer for size and composition analysis of submicron particles, *Aerosol Sci. Tech.*, 33, 49–70, 2000.
- Jimenez, J. L., Jayne, J. T., Shi, Q., Kolb, C. E., Worsnop, D. R., Yourshaw, I., Seinfeld, J. H., Flagan, R. C., Zhang, X., Smith, K. A., Morris, J. W., and Davidovits, P.: Ambient aerosol sampling using the Aerodyne Aerosol Mass Spectrometer, *J. Geophys. Res.-Atmos.*, 108, 8425–8437, doi:10.1029/2001JD001213, 2003.
- Jimenez, J. L., Canagaratna, M. R., Donahue, N. M., Prevot, A. S. H., Zhang, Q., Kroll, J. H., DeCarlo, P. F., Allan, J. D., Coe, H., Ng, N. L., Aiken, A. C., Docherty, K. D., Ulbrich, I. M., Grieshop, A. P., Robinson, A. L., Duplissy, J., Smith, J. D., Wilson, K. R., Lanz, V. A., Hueglin, C., Sun, Y. L., Tian, J., Laaksonen, A., T. R., Rautiainen, J., Vaattovaara, P., Ehn, M., Kulmala, M., Tomlinson, J. M., Collins, D. R., Cubison, M. J., Dunlea, E. J., Huffman, J. A., Onasch, T. B., Alfarra, M. R., Williams, P. I., Bower, K., Kondo, Y., Schneider, J., Drewnick, F., Borrmann, S., Weimer, S., Demerjian, K., Salcedo, D., Cottrell, L., Griffin, R., Takami, A., Miyoshi, T., Hatakeyama, S., Shimojo, A., Sun, J. Y., Zhang, Y. M., Dzepina, K., Kimmel, J. R., Sueper, D., Jayne, J. T., Herndon, S. C., Trimborn, A. M., Williams, L. R., Wood, E. C., Kolb, C. E., Baltensperger, U., and Worsnop, D. R.: Evolution of organic aerosol in the atmosphere, *Science*, 326, 1525–1529, 2009.
- Kalberer, M., Paulsen, D., Sax, M., Steinbacher, M., Dommen, J., Prevot, A. S. H., Fisseha, R., Weingartner, E., Frankevich, V., Zenobi, R., and Baltensperger, U.: Identification of polymers as major components of atmospheric organic aerosols, *Science*, 303, 1659–1662, 2004.
- Kanakidou, M., Seinfeld, J. H., Pandis, S. N., Barnes, I., Dentener, F. J., Facchini, M. C., Van Dingenen, R., Ervens, B., Nenes, A., Nielsen, C. J., Swietlicki, E., Putaud, J. P., Balkanski, Y., Fuzzi, S., Horth, J., Moortgat, G. K., Winterhalter, R., Myhre, C. E. L., Tsigaridis, K., Vignati, E., Stephanou, E. G., and Wilson, J.: Organic aerosol and global climate modelling: a review, *Atmos. Chem. Phys.*, 5, 1053–1123, 2005.

- <http://www.atmos-chem-phys.net/5/1053/2005/>.
- Karydis, V. A., Tsimpidi, A. P., and Pandis, S. N.: Evaluation of a three-dimensional chemical transport model (PMCAMx) in the eastern United States for all four seasons, *J. Geophys. Res.-Atmos.*, 112, D14211, doi:10.1029/2006jd007890, 2007.
- Khlystov, A., Wyers, G. P., and Slanina, J.: The steam-jet aerosol collector, *Atmos. Environ.*, 29, 2229–2234, 1995.
- Kostenidou, E., Pathak, R. K., and Pandis, S. N.: An algorithm for the calculation of secondary organic aerosol density combining AMS and SMPS data, *Aerosol Sci. Tech.*, 41, 1002–1010, 2007.
- Koulouri, E., Saarikoski, S., Theodosi, C., Markaki, Z., Gerasopoulos, E., Kouvarakis, G., Makela, T., Hillamo, R., and Mihalopoulos, N.: Chemical composition and sources of fine and coarse aerosol particles in the Eastern Mediterranean, *Atmos. Environ.*, 42, 6542–6550, doi:10.1016/j.atmosenv.2008.04.010, 2008.
- Kouvarakis, G., Vrekoussis, M., Mihalopoulos, N., Kourtidis, K., Rappengluck, B., Gerasopoulos, E., and Zerefos, C.: Spatial and temporal variability of tropospheric ozone (O₃) in the boundary layer above the Aegean Sea (Eastern Mediterranean), *J. Geophys. Res.- Atmos.*, 107, 8137, doi:10.1029/2000JD000081, 2002.
- Kroll, J. H., Smith, J. D., Che, D. L., Kessler, S. H., Worsnop, D. R., and Wilson, K. R.: Measurement of fragmentation and functionalization pathways in the heterogeneous oxidation of oxidized organic aerosol, *Phys. Chem. Chem. Phys.*, 11, 8005–8014, 2009.
- Kulmala, M., Asmi, A., Lappalainen, H. K., Carslaw, K. S., Pöschl, U., Baltensperger, U., Hov, Ø., Brenquier, J.-L., Pandis, S. N., Facchini, M. C., Hansson, H.-C., Wiedensohler, A., and O'Dowd, C. D.: Introduction: European Integrated Project on Aerosol Cloud Climate and Air Quality interactions (EUCAARI) – integrating aerosol research from nano to global scales, *Atmos. Chem. Phys.*, 9, 2825–2841, 2009, <http://www.atmos-chem-phys.net/9/2825/2009/>.
- Lambe, A. T., Miracolo, M. A., Hennigan, C. J., Robinson, A. L., and Donahue, N. M.: Effective rate constants and uptake coefficients for the reactions of organic molecular markers (n-alkanes, hopanes and steranes) in motor oil and diesel primary organic aerosols with hydroxyl radicals, *Environ. Sci. Technol.*, 43, 8794–8800, doi:10.1021/es061878e, 2009.
- Lanz, V. A., Alfarra, M. R., Baltensperger, U., Buchmann, B., Hueglin, C., and Prvt, A. S. H.: Source apportionment of submicron organic aerosols at an urban site by factor analytical modelling of aerosol mass spectra, *Atmos. Chem. Phys.*, 7, 1503–1522, 2007, <http://www.atmos-chem-phys.net/7/1503/2007/>.
- Lanz, V. A., Alfarra, M. R., Baltensperger, U., Buchmann, B., Hueglin, C., Szidat, S., Wehrl, M. N., Wacker, L., Weimer, S., Caseiro, A., Puxbaum, H., and Prevot, A. S. H.: Source attribution of submicron organic aerosols during wintertime inversions by advanced factor analysis of aerosol mass spectra, *Environ. Sci. Technol.*, 42, 214–220, 2008.
- Lanz, V. A., Prévôt, A. S. H., Alfarra, M. R., Mohr, C., DeCarlo, P. F., Weimer, S., Gianini, M. F. D., Hueglin, C., Schneider, J., Favez, O., D'Anna, B., George, C., and Baltensperger, U.: Characterization of aerosol chemical composition by aerosol mass spectrometry in Central Europe: an overview, *Atmos. Chem. Phys. Discuss.*, 9, 24985–25021, 2009, <http://www.atmos-chem-phys-discuss.net/9/24985/2009/>.
- Lee, B.-H., Hildebrandt, L., Kostenidou, E., Riipinen, I., Engelhart, G. J., Donahue, N. M., and Pandis, S. N.: Volatility of organic aerosol sampled during FAME-2008, to be submitted to *Atmos. Chem. Phys. Discuss.*, 2010.
- Lelieveld, J., Berresheim, H., Borrmann, S., Crutzen, P. J., Dentener, F. J., Fischer, H., Feichter, J., Flatau, P. J., Heland, J., Holzinger, R., Korrman, R., Lawrence, M. G., Levin, Z., Markowicz, K. M., Mihalopoulos, N., Minikin, A., Ramanathan, V., de Reus, M., Roelofs, G. J., Scheeren, H. A., Sciare, J., Schlager, H., Schultz, M., Siegmund, P., Steil, B., Stephanou, E. G., Stier, P., Traub, M., Warneke, C., Williams, J., and Ziereis, H.: Global air pollution crossroads over the Mediterranean, *Science*, 298, 794–799, 2002.
- Lipsky, E. M. and Robinson, A. L.: Effects of dilution on fine particle mass and partitioning of semivolatile organics in diesel exhaust and wood smoke, *Environ. Sci. Technol.*, 40, 155–162, 2006.
- Loo, B. W. and Cork, C. P.: Development of a high efficiency virtual impactor, *Aerosol Sci. Tech.*, 9, 167–176, 1988.
- Mathew, B. M., Middlebrook, A. M., and Onasch, T. B.: Collection efficiencies in an Aerodyne aerosol mass spectrometer as a function of particle phase for laboratory generated aerosols, *Aerosol Sci. Tech.*, 42, 884–898, doi:10.1080/02786820802356797, 2008.
- Mihalopoulos, N., Stephanou, E., Kanakidou, M., Pilitsidis, S., and Bousquet, P.: Tropospheric aerosol ionic composition in the Eastern Mediterranean region, *Tellus B*, 49, 314–326, 1997.
- Morgan, W. T., Allan, J. D., Bower, K. N., Highwood, E. J., Liu, D., McMeeking, G. R., Northway, M. J., Williams, P. I., Krejci, R., and Coe, H.: Airborne measurements of the spatial distribution of aerosol chemical composition across Europe and evolution of the organic fraction, *Atmos. Chem. Phys.*, 10, 4065–4083, doi:10.5194/acp-10-4065-2010, 2010.
- Ng, N. L., Canagaratna, M. R., Zhang, Q., Jimenez, J. L., Tian, J., Ulbrich, I. M., Kroll, J. H., Docherty, K. S., Chhabra, P. S., Bahreini, R., Murphy, S. M., Seinfeld, J. H., Hildebrandt, L., DeCarlo, P. F., Lanz, V. A., Prevot, A. S. H., Dinar, E., Rudich, Y., and Worsnop, D. R.: Organic aerosol components observed in worldwide datasets from aerosol mass spectrometry, *Atmos. Chem. Phys.*, in press, 2010.
- NOAA: HYSPLIT (HYbrid Single-Particle Lagrangian Integrated Trajectory) Model, access via NOAA ARL READY Website, <http://www.arl.noaa.gov/ready/hysplit4.html>, NOAA Air Resources Laboratory, Silver Spring, MD, last access: 23 November 2009.
- Paatero, P. and Tapper, U.: Positive Matrix Factorization: a nonnegative factor model with optimal utilization of error estimates of data values, *Environmetrics*, 5, 111–126, 1994.
- Pikridas, M., Bougiatioti, A., Hildebrandt, L., Engelhart, G. J., Kostenidou, E., Mohr, C., Prevot, A. S. H., Kouvarakis, G., Zarnpas, P., Burkhart, J. F., Lee, B.-H., Psichoudaki, M., Mihalopoulos, N., Pilinis, C., Stohl, A., Baltensperger, U., Kulmala, M., and Pandis, S. N.: The Finokalia Aerosol Measurement Experiment – 2008 (FAME-08): an overview, *Atmos. Chem. Phys. Discuss.*, 10, 6641–6679, 2010, <http://www.atmos-chem-phys-discuss.net/10/6641/2010/>.
- Pope, C. A. and Dockery, D. W.: Health effects of fine particulate air pollution: Lines that connect, *J. Air Waste Manage.*, 56, 709–742, 2006.
- Presto, A. A., Miracolo, M. A., Kroll, J. H., Worsnop, D. R.,

- Robinson, A. L., and Donahue, N. M.: Intermediate-volatility organic compounds: A potential source of ambient oxidized organic aerosol, *Environ. Sci. Technol.*, 43, 4744–4749, 2009.
- Robinson, A. L., Donahue, N. M., Shrivastava, M. K., Weitkamp, E. A., Sage, A. M., Grieshop, A. P., Lane, T. E., Pierce, J. R., and Pandis, S. N.: Rethinking organic aerosols: Semivolatile emissions and photochemical aging, *Science*, 315, 1259–1262, 2007.
- Russell, L. M., Pandis, S. N., and Seinfeld, J. H.: Aerosol production and growth in the marine boundary layer, *J. Geophys. Res.-Atmos.*, 99(D10), 20989–21003, 1994.
- Sage, A. M., Weitkamp, E. A., Robinson, A. L., and Donahue, N. M.: Evolving mass spectra of the oxidized component of organic aerosol: results from aerosol mass spectrometer analyses of aged diesel emissions, *Atmos. Chem. Phys.*, 8, 1139–1152, 2008, <http://www.atmos-chem-phys.net/8/1139/2008/>.
- Sciare, J., Bardouki, H., Moulin, C., and Mihalopoulos, N.: Aerosol sources and their contribution to the chemical composition of aerosols in the Eastern Mediterranean Sea during summertime, *Atmos. Chem. Phys.*, 3, 291–302, 2003, <http://www.atmos-chem-phys.net/3/291/2003/>.
- Seibert, P. and Frank, A.: Source-receptor matrix calculation with a Lagrangian particle dispersion model in backward mode, *Atmos. Chem. Phys.*, 4, 51–63, 2004, <http://www.atmos-chem-phys.net/4/51/2004/>.
- Seinfeld, J. H. and Pandis, S. N.: *Atmospheric Chemistry and Physics*, Second Edition ed., John Wiley & Sons, Hoboken, 2006.
- Stohl, A., Hittenberger, M., and Wotawa, G.: Validation of the Lagrangian particle dispersion model FLEXPART against large scale tracer experiments, *Atmos. Environ.*, 32, 4245–4264, 1998.
- Ulbrich, I. M., Canagaratna, M. R., Zhang, Q., Worsnop, D. R., and Jimenez, J. L.: Interpretation of organic components from Positive Matrix Factorization of aerosol mass spectrometric data, *Atmos. Chem. Phys.*, 9, 2891–2918, 2009, <http://www.atmos-chem-phys.net/9/2891/2009/>.
- Volkamer, R., Jimenez, J. L., San Martini, F., Dzepina, K., Zhang, Q., Salcedo, D., Molina, L. T., Worsnop, D. R., and Molina, M. J.: Secondary organic aerosol formation from anthropogenic air pollution: Rapid and higher than expected, *Geophys. Res. Lett.*, 33, L17818, doi:10.1029/2006GL026899, 2006.
- Wilks, D. S.: *Statistical Methods in the Atmospheric Sciences*, International Geophysics Series, edited by: Dmowska, R. and Holton, J. R., Academic Press, Inc., San Diego, 1995.
- Zhang, Q., Alfarra, M. R., Worsnop, D. R., Allan, J. D., Coe, H., Canagaratna, M. R., and Jimenez, J. L.: Deconvolution and quantification of hydrocarbon-like and oxygenated organic aerosols based on aerosol mass spectrometry, *Environ. Sci. Technol.*, 39, 4938–4952, 2005a.
- Zhang, Q., Worsnop, D. R., Canagaratna, M. R., and Jimenez, J. L.: Hydrocarbon-like and oxygenated organic aerosols in Pittsburgh: insights into sources and processes of organic aerosols, *Atmos. Chem. Phys.*, 5, 3289–3311, 2005b, <http://www.atmos-chem-phys.net/5/3289/2005/>.
- Zhang, Q., Jimenez, J. L., Canagaratna, M. R., Allan, J. D., Coe, H., Ulbrich, I., Alfarra, M. R., Takami, A., Middlebrook, A. M., Sun, Y. L., Dzepina, K., Dunlea, E., Docherty, K., DeCarlo, P. F., Salcedo, D., Onasch, T., Jayne, J. T., Miyoshi, T., Shimojo, A., Hatakeyama, S., Takegawa, N., Kondo, Y., Schneider, J., Drewnick, F., Borrmann, S., Weimer, S., Demerjian, K., Williams, P., Bower, K., Bahreini, R., Cottrell, L., Griffin, R. J., Rautiainen, J., Sun, J. Y., Zhang, Y. M., and Worsnop, D. R.: Ubiquity and dominance of oxygenated species in organic aerosols in anthropogenically-influenced Northern Hemisphere midlatitudes, *Geophys. Res. Lett.*, 34, L13801, doi:10.1029/2007gl029979, 2007.